



HAL
open science

Microfluidic-based chemical absorption technology for CO₂ capture: Mass transfer dynamics, operating factors and performance intensification

Hao Cheng, Yilin Fan, Dominique Tarlet, Lingai Luo, Zhiwei Fan

► **To cite this version:**

Hao Cheng, Yilin Fan, Dominique Tarlet, Lingai Luo, Zhiwei Fan. Microfluidic-based chemical absorption technology for CO₂ capture: Mass transfer dynamics, operating factors and performance intensification. *Renewable and Sustainable Energy Reviews*, 2023, 181, pp.113357. 10.1016/j.rser.2023.113357 . hal-04111231

HAL Id: hal-04111231

<https://hal.science/hal-04111231>

Submitted on 31 May 2023

HAL is a multi-disciplinary open access archive for the deposit and dissemination of scientific research documents, whether they are published or not. The documents may come from teaching and research institutions in France or abroad, or from public or private research centers.

L'archive ouverte pluridisciplinaire **HAL**, est destinée au dépôt et à la diffusion de documents scientifiques de niveau recherche, publiés ou non, émanant des établissements d'enseignement et de recherche français ou étrangers, des laboratoires publics ou privés.

Microfluidic-based chemical absorption technology for CO₂ capture: Mass transfer dynamics, operating factors and performance intensification

Hao CHENG¹, Yilin FAN^{1,*}, Dominique TARLET¹, Lingai LUO^{1,†}, Zhiwei FAN²

¹ Nantes Université, CNRS, Laboratoire de thermique et énergie de Nantes, LTeN, UMR 6607, 44000 Nantes, France

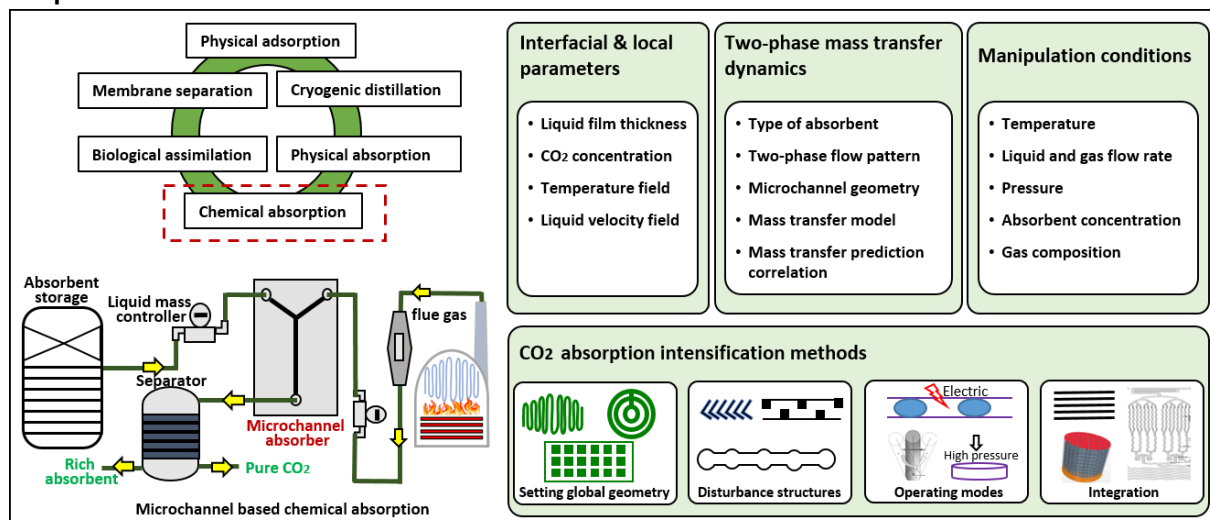
² Shanghai Jiao Tong University Sichuan Research Institute, Chengdu 610213, China

Abstract

Carbon capture, utilization, and storage (CCUS) is a crucial strategy for achieving CO₂ emission reduction targets and mitigating the impacts of global warming and climate change. Among various CCUS technologies, chemical absorption of CO₂ has proven to be a mature and widely-used technique in various industrial sectors. However, the current CO₂ chemical absorption process involves large-scale equipment with low efficiencies, making it difficult to control. To address these issues, microfluidic devices have emerged as a promising technology to intensify the CO₂ absorption process by providing a smaller required volume, enhanced mass transfer, cleaner and safer operations, higher productivity, and more efficient energy use.

This paper aims at presenting a comprehensive literature review on research advances of the microfluidic technology for CO₂ chemical absorption. The review covers various aspects, including microchannel geometries, two-phase flow patterns, mass transfer models, effects of operating factors, and measures to intensify the CO₂ absorption process. In addition, the paper discusses the measurement of interfacial and local parameters, such as liquid film thickness, velocity field, and local CO₂ concentration, which are primordial for understanding the transport phenomena and for optimizing the CO₂ absorbers. This paper may serve as an essential reference that contributes to the development and exploitation of highly-efficient microfluidic-based CO₂ chemical absorption technology for future large-scale industrial applications

Graphical abstract



*Corresponding author: Email: yilin.fan@univ-nantes.fr

†Corresponding author: Email: lingai.luo@univ-nantes.fr

Highlights

- Recent researches on microfluidic-based CO₂ chemical absorption are reviewed.
- Absorption performance is determined by the mass transfer between CO₂ and absorbent.
- Effects of influencing operational factors are discussed.
- Optical techniques are frequently used to measure local & interfacial parameters.
- Different techniques used to intensify the CO₂ absorption process are surveyed.

Keywords:

Carbon capture; CO₂ chemical absorption; Microchannel; Gas-liquid two-phase flow; Mass transfer enhancement; Emission targets

Nomenclature

Latin letters		Abbreviations	
a	Specific surface area, 1/m	CCUS	Carbon Capture, Utilization and Storage
A	Liquid – gas contact area, m ²	CFD	Computational fluid dynamics
C	Concentration, mol/m ³	ECBM	Enhanced Coal Bed Methane
C_e	CO ₂ equilibrium concentration, mol/m ³	IGCC	Integrated gasification combined cycle
d_h	Hydraulic diameter, m	IL	Ionic liquids
D_{diff}	Diffusion coefficient, m ² /s	LFT	Liquid film thickness
E	Enhancement number	LIF	Laser induce fluorescence
g	Gravitational acceleration, m/s ²	LFDM	Laser focus displacement meter
He	Henry constant, Pa.m ³ /mol,	M	mol/L
h	Microchannel height, m	Mn-PTV	Nano-particle tracking velocimetry
i	Amount of bubble in microchannel	PIV	Particle image velocimetry
K_G	Overall gas phase based mass transfer coefficient, kmol /kPa.m ² .h	PTV	Particle tracking velocimetry
k_G	Gas side mass-transfer coefficient, m/s	TPMS	Triply periodic minimum surface
k_L	Liquid side mass transfer coefficient, m/s	VOF	Volume of fluid
k_L^0	Physical mass transfer coefficient, m/s	AEEA	Aminoethylethanolamine
k_{ov}	Overall chemical reaction rate, 1/s	AMP	Aminomethylpropanol
L	Length, m	BDA	1,4 butanediamine
n	Molar flow rate, kmol/h	CO ₂	Carbon dioxide
n_i	Fitting constants	CH ₄	Methane
N	Molar flux, kmol/m ² .h	ChCl	Choline chloride
p	Absorption pressure, kPa	DEA	Diethanolamine
Δp_F	Friction pressure drop, kPa	DAB	1,4-diamidiniumbenzene
Q	Volumetric flow rate, m ³ /s	DEEA	Diethylaminoethanol
R	Gas constant, J/(K.mol)	DMEA	Dimethylethanolamine
r	Radius of bubble in rectangular corner, m	EG	Ethylene glycol
S	Channel cross-section area, m ²	HMDA	Hexanediamine
T	Experimental temperature, K	NHD	Polyethylene glycol dimethylether
U	Superficial velocity, m/s	NaOH	Sodium hydroxide
u	Local flow velocity, m/s	MEA	Monoethanolamine
V	volume, m ³	MDEA	2-(Dimethylamino)ethanol
w	Microchannel width, m	PZ	Piperazine
y	Molar fraction	TEA	Triethanolamine
Y_{CO_2}	CO ₂ loading rate, mol/mol	SDS	Sodium dodecyl sulfate
z	Relative position in flow direction, m		
Greek letters		Dimensionless numbers	
η_{CO_2}	CO ₂ deduction efficiency	Ca	Capillary number, $Ca = \mu U / \sigma$
δ	Liquid film thickness, m	Da	Damköhler number, $Da = k_{ov} \cdot d_h^2 / D$
τ	Gas-liquid contact time, s	Re	Reynolds number, $Re = \rho U d_h / \mu$
ρ	Fluid density, kg/m ³	We	Weber number, $We = \rho U^2 d_h / \sigma$
μ	Dynamic viscosity, Pa.s	Sc_L	Schmidt number, $Sc_L = \mu / \rho D_{CO_2}$
σ	Two-phase interface tension, N/m	Sh_L	Sherwood number, $Sh_L = k_L d_h / D_{CO_2}$
β	Dimensionless structure parameter	Bo	Bond numbers, $Bo = \Delta \rho g d_h^2 / \sigma$
Subscripts/superscripts			
G	Gas	b	Bubble
L	Liquid	e	Equilibrium
in	Inlet	F	Friction
out	Outlet	TP	Two-phase
c	Channel	0	Initial state

1. Introduction

The rapid development of the world economy has been at the large expense of fossil energy resources, resulting in the deterioration of ecology and environment. Researches[1,2] show that the main reason for the global warming during the past 50 years is related to the increased emission of greenhouse gases (GHGs) originated from human activities, such as industrial production, transportation, electricity generation, and homes & commercial businesses. CO₂ is the main GHG and its global monthly mean concentration has increased rapidly from 340 ppm in year 1980 to around 419 ppm in July 2022[3]. The disastrous consequences of global warming due to excessive (CO₂) emissions have been well-recognized, including drought, flood and extreme storm[4]. Since then, the carbon reduction has become an international consensus[5], evidenced by the signing of the Paris Agreement in year 2015[6]. In order to reach the 2050 carbon neutrality (net-zero) target [7], significantly increasing efforts have been devoted to the development and exploitation of Carbon Capture, Utilization and Storage (CCUS)-related technologies (cf. Fig.1) to balance the CO₂ emissions with its removal[8,9].

As the basic and indispensable step of CCUS process, the development of efficient and low energy-consuming CO₂ capture technologies has long become the research focus[5]. Conventional CO₂ capture methods include chemical absorption, physical absorption or adsorption, membrane separation, cryogenic distillation, biological assimilation and others[10,11]. Their basic operation principles, advantages and disadvantages are summarized and compared in Table 1.

Among these CO₂ capture technologies, the cryogenic distillation is featured by the maturity and high capture efficiency, but involving high equipment investment and intensive energy consumption. The biological assimilation is much natural, environment-friendly and low energy input. But the slow process and limited scalability hinder its large-scale industrial application. The capture efficiency of physical adsorption and membrane separation depends strongly on the physical properties of material, and usually the recycling of these materials is a real problem. Compared with the above-mentioned methods, the chemical absorption seems to be the most adapted and widely used one for large-scale industrial applications[12,13]. This method uses chemical solvent(s) to react with the CO₂; the absorbed gas could then be released by heating the product for the downstream processing (storage or utilization). It is a mature technology featured by high CO₂ selectivity, low solvent consumption and high cost-effectiveness. Therefore, it has covered the CO₂ capture market of coal-fired power plants accounting for 60% of the global capacity[14]. Over the past few decades, the large-scale absorption equipment such as absorption tower has played a very important role in industry CO₂ capture, featured by many advantages such as simple process control and stable equipment operation. However, the use of such large-scale equipment inevitably brings problems like high investment costs, excessive amount of solvent needed, high energy consumption, large occupied space and additional security measures, thereby hindering its further market development. One of the promising solutions to solve the above-mentioned drawbacks is through the process miniaturization, i.e., by the employment and implementation of microfluidic devices.

Microfluidic-based CO₂ capture is a technology developed to control and manipulate the CO₂ (gas) absorption process by a chemical solvent (liquid) in miniaturized absorbers/reactors with channel characteristic size in the order of micro or millimeter. Numerous studies have shown that the gas-liquid two-phase flow in microchannel reactors, when properly configured and handled, could exhibit numerous interesting features, including enhanced mass transfer due to high volumetric interfacial surface area, better repeatability and stability, safe manipulation with low leakage risk, and easy upscaling by the numbering-up[15,16]. The microfluidic technology has already been applied in many industrial fields, including medicine and pharmaceutical analysis[17–19]. Using microchannel reactors for CO₂ chemical absorption is also considered as a promising alternative technology pathway of macro-sized conventional equipment.

Table 1. Summary of conventional CO₂ capture technologies.

Technology	Definition & Operation principle	Advantages	Disadvantages	Application fields	Performance indicators*	Refs.
Chemical absorption	Using a solvent to absorb CO ₂ from flue gas or other industrial emissions	<ul style="list-style-type: none"> - High contact surface area, high capture efficiency and selectivity; - Mature technology; - Low investment cost; - Low carbon leakage; - Standardized and easy process control. 	<ul style="list-style-type: none"> - Corrosive; - High energy consumption; - Chemical solution post-treatment. 	<p>Large-scale coal-fired power plants and other fossil energy based industries</p> <p>Large-scale energy conversion stations, such as integrated gasification combined cycle (IGCC) power plants, natural gas processing, coal chemical industry, etc.</p>	<p>$\eta_{CO_2} > 90\%$;</p> <p>Energy consumption: 1-3 GJ/t(CO₂);</p> <p>Cost: 10-50 \$/t(CO₂).</p>	[20,21]
Physical absorption	Dissolving CO ₂ in a liquid at high pressure and low temperature	<ul style="list-style-type: none"> - Cheap absorbent; - Mature technology; - High security. 	<ul style="list-style-type: none"> - Low selectivity; - Slow process; - Extra high energy consumption. 	<p>Ammonia synthesis, hydrogen production, natural gas treatment, etc.</p>	<p>$\eta_{CO_2} > 90\%$</p>	[22]
Physical adsorption	Using solid material to adsorb CO ₂ from flue gas or other industrial emissions by intermolecular forces	<ul style="list-style-type: none"> - High contact area, high capture efficiency; - Mature technology; - High security; - Simple process. 	<ul style="list-style-type: none"> - Low selectivity; - Low carbon loading rate of solid adsorbent; - Low adsorption flux; - Low material recovery; - Energy-intensive carbon separation. 	<p>Small waste heat recovery plant, biomass power plant</p>	<p>$\eta_{CO_2} > 85\%$</p>	[23,24]
Membrane separation	Using a membrane to selectively separate CO ₂ from flue gas or other industrial emissions	<ul style="list-style-type: none"> - High selectivity; - High CO₂ purity; - Low energy consumption. 	<ul style="list-style-type: none"> - High processing cost; - Recycling of membranes; - Larger flux resistance. 	<p>IGCC power plants</p>	<p>$\eta_{CO_2} > 90\%$;</p> <p>- Energy consumption: 0.01-0.04 GJ/t(CO₂).</p>	[25,26]
Cryogenic distillation	Separating CO ₂ from flue gas or other industrial emissions using low-temperature distillation	<ul style="list-style-type: none"> - Mature technology; - High selectivity; - Low CO₂ transport cost. 	<ul style="list-style-type: none"> - Large-scale equipment investment; - Intensive energy consumption to maintain the low temperature. 	<p>Biofuel production, soil pollution bioremediation</p>	<p>$\eta_{CO_2} > 98\%$;</p> <p>Energy consumption: 2.4 GJ/t(CO₂).</p>	[27,28]
Biological assimilation	Using plants and other photosynthetic organisms to absorb CO ₂ and convert it into organic compounds.	<ul style="list-style-type: none"> - Low energy requirements; - Natural process; - Potential for carbon sequestration. 	<ul style="list-style-type: none"> - Limited scalability; - Slow process; - Strong environmental dependence. 	<p>Absorption efficiency depends on environment and biological species; No requirement of external energy inputs</p>	<p>[29–31]</p>	

*CO₂ deduction efficiency: $\eta_{CO_2} = \frac{y_{CO_2}^{in} - y_{CO_2}^{out}}{y_{CO_2}^{in}}$, where $y_{CO_2}^{in}$ is CO₂ molar fraction before entering the reactor, $y_{CO_2}^{out}$ is CO₂ molar fraction after absorption.

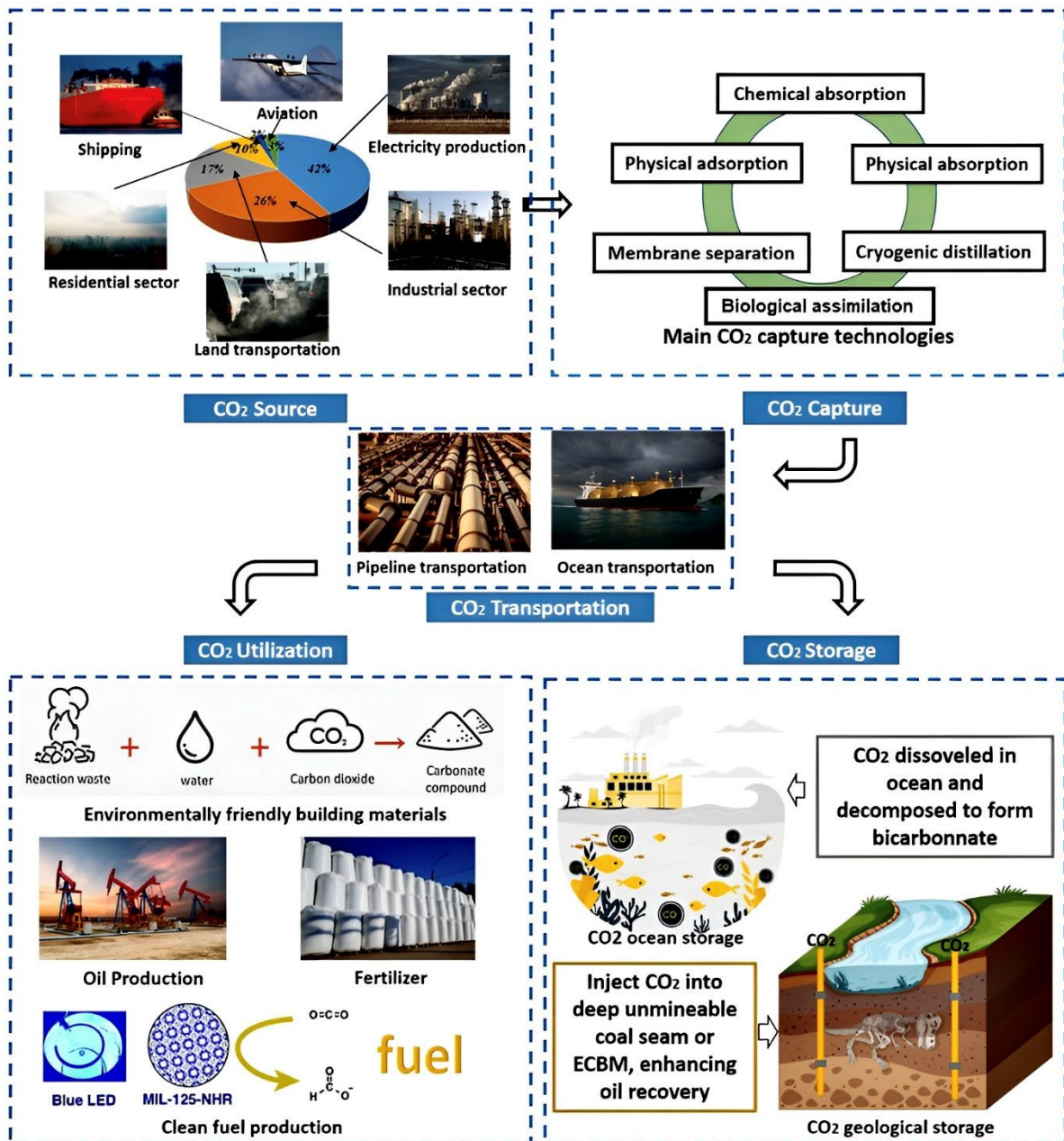


Figure 1 CCUS flow chart and related technologies. (Data of CO₂ source from [1])

The microfluidic-based CO₂ absorption has long been the hot spot of the CCUS research community. In literature, a great number of researches have been focused on developing adapted absorbents[32–34] with expected features such as high CO₂ selectivity, stable, low corrosive, low toxicity and non-flammable. The two-phase flow patterns in microchannel and suitable working conditions for CO₂ absorption have also been broadly investigated[35–38]. Different mass transfer models have been proposed and developed to characterize and predict the CO₂ absorption performance in various absorbents[39]. Moreover, extensive research efforts have been devoted to the micro reactor design and structure optimization with the aim of mass transfer intensification[35,40–42], other researchers focus on multi-phase mass transfer process in micro reactor, such as Yao et al.[43] reviewed in detail the two-phase mass transfer mechanism and dynamics, but lack of the specific application on CO₂

absorption. Relevant reviews have also been published, as summarized in Table 2. Nevertheless, some of them are focused on the absorbents for CO₂ capture[44], with special focus on calcium oxide[45], potassium carbonate[46], ionic liquids[47], biphasic solvents[48], etc., while others try to review the factors affecting CO₂ absorption, such as absorber structure, dimensions, operational temperature, pressure, etc., but more focused at the macroscopic scale[49,50]. Recently, Afzal et al.[42] presented a comprehensive review on the microchannel geometry, fabrication methods and applications in prospective industries. Noteworthy is the recent paper of Pasha et al.[5] reviewing the hydrodynamics and mass transfer characteristics of CO₂ absorption in micro reactors. The two-phase flow patterns, the microreactor designs, the influencing factors and the economic aspect are specially focused and described. Some mass transfer intensification methods were mentioned, but only focusing on the overall structure of the reactor while more attempts on the local structuration were still absent. In brief, a systematic and comprehensive state-of-art literature review to keep track with the relevant studies and new developments on the microchannel CO₂ mass transfer models, the impact of different operating conditions, the measurement of local & interfacial parameters and the process intensification measures is still lacking.

Table 2. Summary of some published reviews related to CO₂ chemical absorption.

Study (year)	Main contents	Key findings
Zhang et al.[45] (2015)	Calcium oxide-based sorbents for CO ₂ capture under high temperature.	Under high temperature, water vapor can augment the humidity which enhances the CO ₂ adsorption capacity of CaO. Detailed mechanism of the influence of steam during carbonation remains to be clarified.
Mumford et al.[44] (2015)	Solvent-based CO ₂ capture technologies, and insight on the new CO ₂ absorption solvent.	Importance of new absorbents and absorber miniaturization is highlighted from the aspects of cost expenditure and absorption efficiency.
Hu et al.[46] (2016)	Potassium carbonate absorbents used for CO ₂ absorption. Reaction efficiency improvement.	Optimum condition of potassium carbonate absorbents is discussed for practical industrial CO ₂ absorption.
Mehdi et al.[51] (2018)	Gas-liquid and liquid-liquid mass transfer in microchannel reactor. Influencing factors on microchannel based mass transfer performance.	Effects of aspect ratio, surface properties of microchannel wall etc. on mass transfer need to be further clarified.
Aghaie et al.[47] (2018)	Current status and future prospects about CO ₂ capture by ionic liquids solvents.	Ionic liquids solvents show good absorption performance and economic advantages. Influence of different parameters are clarified.
Ochedi et al.[50] (2021)	CO ₂ capture based on the liquid absorption methods. Absorption performance, absorption mechanism and challenges.	Phase-change absorbents and absorbents with nanoparticles show great advantages in CO ₂ chemical absorption with low energy consumption.
Yao et al.[43] (2021)	Two-phase flow and mass transfer mechanism in microchannel. Some application cases involving CO ₂ capture.	Microfluidic technology enhances multi-phase reactions owing to the enhanced heat and mass transfer, and enables precise control of the reaction process.

Pasha et al.[5] (2022)	Hydrodynamics, mass transfer characteristics, designs, influencing factors and economic analysis on CO ₂ absorption in micro reactors.	Micro-absorber shows great advantages on CO ₂ absorption with a higher capital expenditure. Parallelized microchannels can augment the capture throughput, but the two-phase misdistribution issue remains to be overcome.
Meng et al.[49] (2022)	Aqueous amine solution for CO ₂ chemical absorption.	Amine scrubbing technology is rather promising for CO ₂ capture; Several issues should be overcome including environment risks and high energy consumption.
Afzal et al.[42] (2022)	Microchannel fabrication methods and applications in large-scale and prospective industries.	Compared with straight microchannel, the fabrication and two-phase flow analyze of sinusoidal microchannel are more complicated and need furtherly investigated.
Gautam & Mondal[48] (2023)	The characteristics, applications and prospects of novel biphasic solvents.	Biphasic solvents are featured by fast reaction kinetics, high absorption capacity, and low regeneration energy required.
This article	Two-phase flow patterns and mass transfer models; Effect of operating parameters on the CO ₂ absorption in microchannel; Identification and measurement of some interfacial & local parameters; Measures to enhance the CO ₂ absorption performance in microchannel-based reactors.	Optimizing the micro-absorber structure can greatly improve the CO ₂ absorption performance and extend the potential for industrial application. The measurement of interfacial and local parameters is a key issue for CO ₂ absorption model building and structure optimization.

This review paper is thereby expected to fill the literature gap by gathering and surveying previous works on the microfluidic-based CO₂ absorption technology, a research topic with rapid progress in recent years. In particular, the paper has the following objectives:

- A combined understanding of basic flow patterns, mass transfer dynamics and microreactor geometries;
- A complete survey on the effects of various operational factors on the CO₂ absorption performance in microchannel, including operating temperature and pressure, gas and liquid velocity, gas composition, and the absorbent concentration;
- A special focus on the local & interfacial parameters (e.g., liquid film thickness, local CO₂ concentration and velocity profiles) and their measurement by experiments, which are firstly documented;
- An overview of the CO₂ absorption performance intensification measures proposed and implemented by different researchers, essential for the applications in large-scale industries of this technology.

This paper may serve as an essential reference that contributes to the development and exploitation of highly-efficient microfluidic-based CO₂ chemical absorption technology for its future application and propagation in different industrial sectors.

2. Fluid flow and mass transfer of CO₂ chemical absorption in microchannel

This section presents basic elements about the microfluidic-based CO₂ chemical absorption process. Since CO₂ is the targeted gas phase, different chemical absorbents have been proposed and used as the liquid phase, including ammonia and its derivatives[52], alkaline[53], amine absorbent blends[54], ionic Liquids functioned absorbents[55] and phase change absorbents[56]. Developing highly-performant chemical absorbent with expected features has become a very important subject in CO₂ chemical absorption, but beyond the scope of this paper. Interested readers are invited to consult ref.[50] for more details.

2.1 Two-phase flow patterns for CO₂ absorption in microchannel

The gas-liquid two-phase flow pattern plays a determinant role on the mass transfer characteristics of CO₂ chemical absorption in microchannel. Basic flow patterns identified for CO₂ chemical absorption in microchannel include bubbly flow, slug (Taylor) flow, slug-annular flow, and churn flow. Detailed description and illustration of these flow patterns may refer to the review paper[5]. Some other specific flow patterns have also been reported, such as slug-bubbly flow, distorted Taylor flow, complete and partial bubble break flow, etc.[57–59]. Most of them are linked to the channel structuration and will be introduced in the later section 5.2.

Two-phase flow maps are then constructed to better predict and determine the flow regimes in microchannel and their possible transition within a certain range of working conditions. Common flow maps use superficial velocity (U) or Weber number (We) of the gas and liquid phase as coordinates, each flow pattern occupying a specific region on the map. Detailed and systematic studies on the basic two-phase flow maps in microchannel may be found in ref.[60]. Specially for CO₂ absorption, the chemical reaction rate would affect the shift of regime transitions under certain conditions[61,62].

Among the above mentioned common flow patterns, the slug flow (Taylor flow) seems to be the most suitable one for microchannel-based CO₂ absorption because of the stable gas-liquid mass transfer interface, simple manipulation and easy controllability. As a result, it has received much attention and has been widely used in relevant researches reported in the literature (cf. Table 3).

2.2 Microchannel geometry

The fabrication method of microchannels, such as photolithography, soft lithography, or micromachining[63], can be used to set the geometry of microchannel absorber such as size, cross-sectional shape & junction type. These geometry parameters have been found to have a significant influence on the two-phase flow patterns which is essential for the CO₂ chemical absorption. The hydraulic diameter (d_h) of the microchannel used for CO₂ absorption is usually between 200 μm and 1000 μm , with a cross-sectional shape of circular, rectangular, square, triangle, trapezoid, etc. (Fig.2a). The length of microchannel (L_c) used for CO₂ absorption study in laboratory is usually shorter than 400 mm depending on the visualization window of the instruments. More details of microchannel geometry are summarized in Table 3.

The cross-sectional shape of microchannel directly affects the distribution of liquid film thickness (LFT) between the gas phase and the wall, thereby influencing the generation and the moving of Taylor

bubbles[64]. Choi et al.[65] reported the increased Taylor bubble velocity with the decreasing aspect ratio of the cross-section due to the corner effect. Cantu-Perez et al.[66] numerically investigated the effect of sectional shapes (e.g., flat, circle-arc etched, rectangular-shape etched and V-shape etched) on the CO₂ absorption by NaOH solution. They demonstrated much more stable flow pattern in flat rectangular shape microchannel because of the thin, spatially uniform and stable liquid film caused by corner capillary effect. For better visualization purpose, flat rectangular micro-channels become more frequently used for CO₂ chemical absorption experiments.

The microchannel size directly influences the energy dissipation of whole CO₂ absorption process[67–69]. Yue et al.[70] experimentally demonstrated that the increased pressure drop (caused by smaller d_h) promoted the slug flow pattern in a much larger gas velocity range. Ganapathy et al.[71] demonstrated that the mass transfer rate could also be strengthened, e.g., liquid side volume mass transfer coefficient ($k_L a$) increased by 2.6 times when the microchannel size decreased from 762 μm to 254 μm .

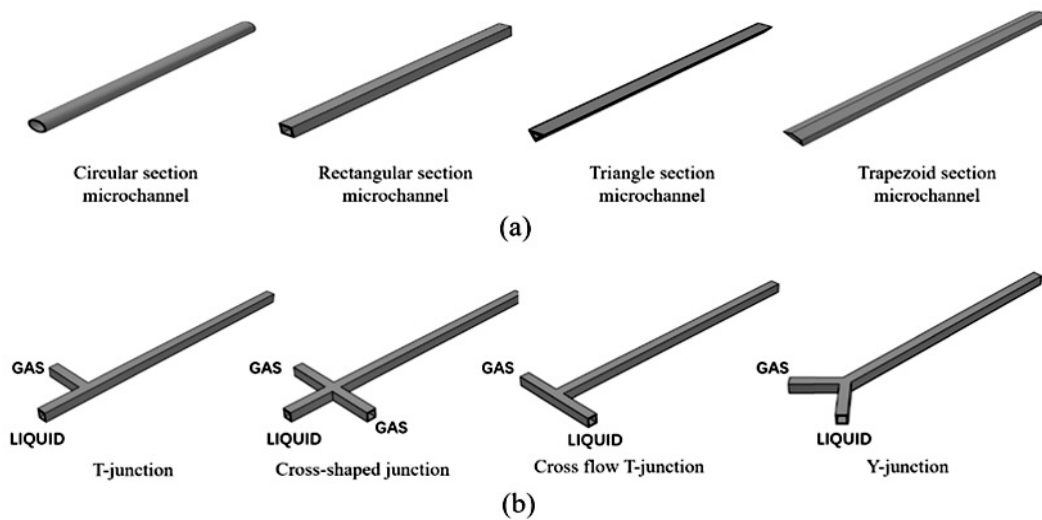


Figure 2 Conventional cross-section shapes and junction types of microchannel reactor for CO₂ chemical absorption

Many researchers have reported that the junction (mixing) structure could directly affect the gas phase bubble generation and growth in the microchannel. The most widely used junction types include T-junction, Y-junction, cross-junction, etc. (Fig.2b). It has been reported that the blocking-squeezing mechanism of T-junction at low liquid flow rate could generate stable bubble and Taylor flows[72,73], therefore preferred for microchannel-based CO₂ absorption experiments (cf. Table 4). Tan et al.[74] tested the mass transfer rate of different gas-liquid inlet angle (60°-150°) for a rectangular microchannel and verified that the T-junction rendered better mass transfer performance because of the highest shear force. This conclusion has been confirmed by numerous experimental studies in the literature[75–77]. Instead of straight microchannel, other channel settings (spiral, serpentine, etc.) have also been proposed and tested, in view of intensifying the CO₂ absorption. This aspect will be further introduced in the later section 5.1.

2.3 Mass transfer model

In this section, some basic mass transfer models for CO₂ absorption in microchannel are introduced. The schematic for some mass transfer models are shown in Fig.3.

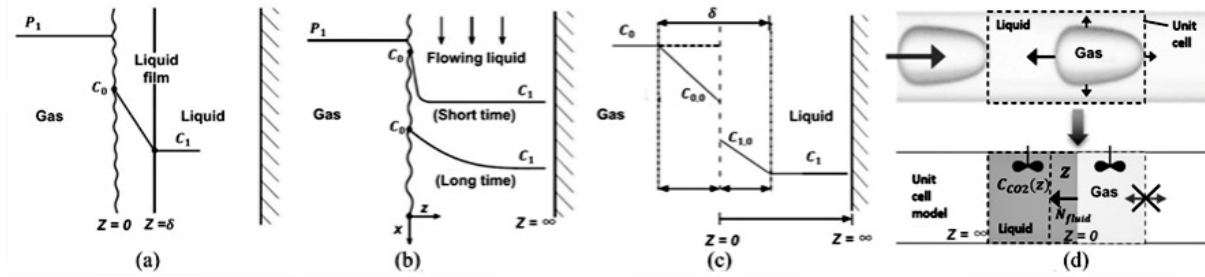


Figure 3 Schematic of mass transfer model. (a) Thin film mass transfer model. (b) Penetration mass transfer model. (c) Two film mass transfer model. (d) Unit-cell model. Adapted with permission from Ref. [78], copyright (2020) Elsevier

2.3.1 Thin film model

Thin-film (or stagnant-film) model[79] (Fig.3a) assumes that a thin stagnant liquid film exists for stable gas molecular diffusion into the liquid phase. This model fits the condition that the gas and liquid phases are stable, or the diffusion through the film caused by concentration difference dominates the mass transfer. The basic overall mass transfer rate can be expressed as:

$$n_{0-1} = kA(C_0 - C_1) \quad (1)$$

Where n_{0-1} (kmol/h) is the molar flow rate, A (m²) is the gas-liquid contact area, k is the mass transfer coefficient, C_0 and C_1 (mol/L) are the solution concentration at the contact surface and the bulk solution, respectively. k could be described by the Fick's first law:

$$n_{0-1} = \frac{D_{diff}}{\delta} A(C_0 - C_1) \quad (2)$$

Where δ is the thin film thickness, D_{diff} is the diffusion coefficient. Although this model can characterize some features of the real mass transfer process in a simple way, the prediction or determination of δ is sometimes difficult because it depends on the reactor geometry, two-phase flow pattern and physical properties (e.g., viscosity, density, etc.). Besides, significant error may occur for mass transfer prediction, especially when convection-based mass transfer cannot be neglected.

2.3.2 Penetration model

Penetration model (Fig.3b)[79,80] are based on two assumptions: (1) a fixed hypothetical diffusion layer at steady-state mass transfer; (2) the diffusion-dominated mass transfer in the perpendicular direction to the interface whereas the convection-dominated mass transfer in the liquid flowing direction.

n_{0-1} for CO₂ absorption can be written as Eq. (3), and the liquid-phase mass transfer coefficient can be expressed using the Crussler formula[81]:

$$n_{0-1} = 2 \sqrt{\frac{D_{diff}}{\pi\tau}} A(C_0 - C_1) \quad (3)$$

$$k_L = 2 \sqrt{\frac{D_{CO_2}}{\pi\tau}} \quad (4)$$

Where τ is the gas-liquid contact time calculated by:

$$\tau = \frac{3600whL_c}{Q_G + Q_L} \quad (5)$$

Q_G and Q_L is the volumetric flow rate for the gas and liquid phase, respectively. w , h , L_c is width, height and length of channel respectively. D_{CO_2} is the CO₂ diffusion coefficient in the chemical absorbent.

2.3.3 Two-film model

The two-film model[82,83] (Fig.3c) assumes a gas stagnation layer (gas film) and a liquid stagnation layer (liquid film) on each side of the gas-liquid interface. CO₂ molecules are firstly transported to the two-phase interface and then dissolved in the liquid phase due to the partial pressure differences. Finally, the CO₂ required for chemical reaction is ready and begins to react with the liquid absorbent. The molar flux of volumetric mass transfer $N_{CO_2}a$ (kmol/m³h) can be calculated as Eq. (6) based on the mass conservation:

$$N_{CO_2}a = \frac{n}{V_c} (y_{CO_2}^{in} - y_{CO_2}^{out}) \quad (6)$$

Where V_c (m³) is reaction section volume of the micro reactor (such as microchannel) and N_{CO_2} (kmol/m².h) is the molar flux. For stable two-phase slug flow, the gas-liquid specific surface area (a) of a single long bubble can be calculated as:

$$a = \frac{\pi w^2 + [2\pi r + 4(w - 2r)](L_b - w)}{V_c} \quad (7)$$

Where L_b is the length of single bubble, r is the average radius of bubble cross-section.

$N_{CO_2}a$ can also be expressed as the product of a mass transfer coefficient and the corresponding driving force[84], such as:

$$N_{CO_2}a = K_G a p (y_{CO_2}^G - y_{CO_2}^*) \quad (8)$$

Where p (kPa) is absorption pressure, K_G (kmol/kPa.h.m²) is the overall gas phase-based mass transfer coefficient, $y_{CO_2}^G$ and $y_{CO_2}^*$ is the molar fraction of CO₂ in the gas phase and at two-phase interface, respectively. $y_{CO_2}^*$ is near-zero because of the instantaneous reaction between CO₂ molecular and absorbent molecular in the liquid phase[85]. As a result, Eq. (8) can be simplified as:

$$N_{CO_2}a = K_G a p y_{CO_2}^G \quad (9)$$

$y_{CO_2}^G$ is not a constant but varies along with the position of bubble. In practice, the average value of $y_{CO_2}^G$ between the inlet and outlet of the microchannel is often used:

$$y_{CO_2}^G = \frac{y_{CO_2}^{in} - y_{CO_2}^{out}}{\ln\left(\frac{y_{CO_2}^{in}}{y_{CO_2}^{out}}\right)} \quad (10)$$

$K_G a$ can then be expressed by:

$$K_G a = \frac{N_{CO_2} a}{p} \left(\frac{\ln\left(\frac{y_{CO_2}^{in}}{y_{CO_2}^{out}}\right)}{y_{CO_2}^{in} - y_{CO_2}^{out}} \right) \quad (11)$$

N_{CO_2} can also be expressed by liquid side mass-transfer coefficient in stable CO₂ absorption process, written as:

$$N_{CO_2} = k_L (C_e - C) \quad (12)$$

Where k_L (m/s) is the liquid side mass-transfer coefficient, C is the CO₂ concentration in liquid equaling to 0 because of complete chemical reaction. C_e is the CO₂ equilibrium concentration at the interface, expressed as Eq. (13) according to Henry's law[86]:

$$C_e = p_{CO_2} / He \quad (13)$$

Where He (Pa.m³/mol) is Henry constant and decided by dissolution type and temperature. p_{CO_2} is the average CO₂ gas pressure in microchannel. The CO₂ molar quantity of whole bubble absorbed into the liquid in the main channel can be expressed as:

$$i * n_{gas} = \frac{p_{in} V_{in} - p_{out} V_{out}}{RT} \quad (14)$$

Where R is the gas constant, T is the experimental temperature and i is the number of bubbles in the microchannel. N_{CO_2} and k_L can then be calculated as:

$$N_{CO_2} = \frac{i * n_{gas}}{a} = \frac{(p_{in} V_{in} - p_{out} V_{out})}{aRT} \quad (15)$$

$$k_L = \frac{N_{CO_2}}{C_e} = \frac{(p_{in} V_{in} - p_{out} V_{out}) He}{aRT p_{CO_2}} \quad (16)$$

2.3.4 Unit-cell model

The unit-cell model[78] (Fig.3d) is based on five main hypotheses: (1) no mass transfer between unit-cells; (2) concentration equilibrium at gas-liquid interface; (3) mass transfer only from gas phase to liquid phase; (4) same velocity of gas phase and liquid phase; and (5) constant liquid side volume mass transfer coefficient along the microchannel. The CO₂ concentration variation along the two phase motion direction (z -direction in Fig.3d) can be written as follows:

$$\frac{dC_{CO_2}}{dz} = \frac{k_L a_L}{U_{TP}} (C_e - C_{CO_2}(z)) \quad (17)$$

Where U_{TP} is the two phase flow velocity calculated as:

$$U_{TP} = \frac{Q_G + Q_L}{S} = \frac{dz}{dt} \quad (18)$$

S (m²) is the microchannel cross-section area and z is the length from the supposed gas-liquid interface ($z=0$) to the calculation point. The $k_L a$ along z direction can be expressed as:

$$k_L a(z) = \frac{U_{TP}}{z} \ln\left(\frac{C_e - C_{CO_2}(z=0)}{C_e - C_{CO_2}(z)}\right) \quad (19)$$

A key information for this model is the CO₂ concentration in liquid slug, which can be measured by many ways such as Raman spectra measurement[78]. More information about the CO₂ concentration measurement can be found in section 4.2 of this paper.

2.3.5 Hydrodynamic model

Under the elevated system pressure, calculation methods based on the bubble volume may be no longer well suited because of the deviation from ideal gas assumption. Some simplified hydrodynamic models were proposed. For example, Jepsen[87] proposed the energy dissipation model as follows:

$$k_L a = \frac{\Delta p_F}{L_c} (U_G + U_L) \quad (20)$$

Where Δp_F is the inlet-outlet pressure drop caused by flow friction in microchannel. Yue et al.[88] studied the mass transfer process of the CO₂/water system in the microchannel and proposed a simplified model with fewer parameters:

$$k_L a = 0.0863 \left(\frac{\Delta p_F}{L_c}\right)^{0.881} \quad (21)$$

Nevertheless, Guo et al.[89] pointed out that the average deviation between the predicted value and the experimental value could reach about 40%, the model correction is thereby needed. Yang et al.[90] proposed to include U_G , U_L and E (the enhancement coefficient of chemical reaction rate on mass transfer) in the model:

$$k_L a = n_1 \left(\frac{\Delta p_F}{L_c}\right)^{n_2} (U_G + U_L)^{n_3} E^{n_4} \quad (22)$$

$$E = \frac{k_L}{k_L^0} \quad (23)$$

Where k_L^0 is the physical mass transfer coefficient in the liquid phase, and n_1 - n_4 are fitting constants by experimental data.

2.3.6 Empirical correlations

Besides the above-mentioned physical models, some empirical correlations have also been proposed for fast estimation and prediction. These correlations usually have the form of liquid side Sherwood number ($Sh_L = k_L d_h / D_{CO_2}$) in relation to other dimensionless numbers such as Re_L , Re_G , Sc_L , Ca , etc. For example, Yue et al.[37] investigated the microchannel based CO₂-H₂O absorption and proposed the correlation for slug flow (Eq. 24) and for slug-annular flow (Eq. 25), respectively.

$$Sh_L \cdot a \cdot d_h = 0.084 Re_G^{0.213} \cdot Re_L^{0.937} \cdot Sc_L^{0.5} \quad (24)$$

$$Sh_L \cdot a \cdot d_h = 0.058 Re_G^{0.344} \cdot Re_L^{0.912} \cdot Sc_L^{0.5} \quad (25)$$

For furtherly investigated the effects of physical parameters on mass transfer performance, Ji et al.[91] tested the mass transfer performance of CO₂/DI water, CO₂/ethanol and CO₂/n-propanol in 40 μm×240 μm, 100 μm×800 μm and 100 μm×2000 μm rectangular microchannels within Re_L (1.1 – 13.07) and Re_G (0.87 – 61.9). Eq. (26) was put forward for Taylor bubble flow and annular flow:

$$Sh_L \cdot a \cdot d_h = 0.22 Re_G^{0.78} \cdot Re_L^{0.0535} \cdot Sc_L \cdot Ca_L^{0.7586} \quad (26)$$

For predicting the chemical reaction accompanied mass transfer performance, Niu et al.[92] investigated the CO₂/N₂-NHD system in a circular microchannel ($d_h=1$ mm). Eq. (27) was obtained to predict the mass transfer performance within the range of U_L (0.03 – 0.9 m/s) and U_G (0.03 – 9.98 m/s):

$$Sh_L \cdot a \cdot d_h = 0.116 Re_G^{0.39} \cdot Re_L^{0.7} \cdot Sc_L^{0.5} \quad (27)$$

Li et al.[93] experimentally investigated the CO₂/MEA solution mass transfer performance in a 400 μm×600 μm rectangular microchannel under Taylor flow and annular flow pattern ($26.73 < Re_G < 467.79$ and $5.35 < Re_L < 37.42$). Two empirical correlations were proposed with a maximum error of 8.91% and 4.73% for small and large Re_G/Re_L , respectively.

$$Sh_L \cdot a \cdot d_h = 5.0107 Re_G^{2.9423} \cdot Re_L^{-1.5583} \cdot Sc_L^{0.5} \cdot Ca_L^{0.0743} \quad \frac{Re_G}{Re_L} < 1.7319 \quad (28)$$

$$Sh_L \cdot a \cdot d_h = 19.3895 Re_G^{0.3872} \cdot Re_L^{0.8865} \cdot Sc_L^{0.5} \cdot Ca_L^{0.4176} \quad \frac{Re_G}{Re_L} \geq 1.7319 \quad (29)$$

However, these prediction correlations are only based on physical parameters and for a specific microchannel geometry. Large discrepancy may occur when predicting CO₂ chemical absorption in microchannel. For this issue, Yin et al.[94] introduced the Da number to characterize the effect of chemical reaction on mass transfer:

$$Sh_L \cdot a \cdot d_h = 0.81 \cdot Re_G^{0.78} \cdot Re_L^{0.41} \cdot Da^{0.35} \quad (30)$$

Where Da is the Damköhler number ($Da = k_{ov} \cdot d_h^2 / D$), and k_{ov} is the overall chemical reaction rate (1/s). Zhang et al.[95] investigated the CO₂ absorbed by sodium glycinate aqueous solution in microchannel and proposed to include the enhancement number E in the correlation:

$$Sh_L \cdot a \cdot d_h = 0.004 \cdot Re_G^{1.262} \cdot Re_L^{0.587} \cdot Sc_L^{0.5} E^{1.1955} \quad (31)$$

$$E = \frac{\sqrt{k_{ov} D}}{k_L^0} \quad (32)$$

The above-mentioned correlations were proposed for smooth straight microchannels. For structured microchannels like non-straight channel and/or with obstacles inside, a corrective factor should be added to take the enhancement effect into account. For example, Chu et al.[96] proposed to add the enhancement number E for a serpentine microchannel (400 μm×400 μm):

$$Sh_L \cdot a \cdot d_h = 1.3425 Re_G^{1.0968} \cdot Re_L^{-0.4705} \cdot Sc_L^{0.5} \cdot Ca_L^{-0.0302} \cdot E^{0.7198} \quad (33)$$

Zhang et al.[59] proposed to add the structure factor β for their microchannel geometry with sudden expansion:

$$Sh_L \cdot a \cdot d_h = 0.084 Re_G^{1.064} \cdot Re_L^{0.422} \cdot Sc_L^{0.5} \cdot \beta^{0.191} \quad (34)$$

A summary of the studies over various microchannel geometries, used absorbents and absorption performances can be found in Table 3.

Table 3 Summary of microchannel-based CO₂ absorption conditions and performances reported in different researches.

Absorbent	Microchannel structure	Size	Flow pattern	Operation condition	η_{CO_2}	k_L (m/s)	$k_L a$ (1/s)	Δp (kPa)	Ref.
NaHCO ₃ /Na ₂ CO ₃	Y-type rectangular	1000 μm ×500 μm $L_c=48$ mm	Slug	U_G : 0.7-13 m/s U_L : 0.09-1 m/s		14.4×10 ⁻⁴	21	24	[37]
DI water	Y-type rectangular, square	$d_h=667, 400, 200$ μm $L_c=48$ mm	bubbly, slug, slug-annular, churn and annular	U_G : 0.04-60 m/s U_L : 0.02-1 m/s					[70]
PZ, MDEA	Cross T-type rectangular	$d_h=500, 1000, 2000$ μm $L_c=180$ mm		U_G : 2-5 m/s U_L :0.02-0.05 m/s	98%			6.1	[97]
MEA	T-type rectangular	400 μm ×600 μm $L_c=45$ mm	Slug, annular	Q_G : 50-875 ml/h Q_L : 10-70 ml/h			0.25-54.94		[93]
DEA	Cross T-type circular	$d_h=762$ μm	Slug	U_G : 1.8-9.1 m/s U_L : 0.04-0.4 m/s	Close to 100%		11-132	10.2	[98]
MDEA+PZ	Microporous tube-in-tube	$d_{out}=15$ mm $d_{in}=15.5, 16, 16.5, 17$ mm $d_{micropore}=5, 10, 20, 40, 80$ μm	Annular	Q_G : 0-5.32 × 10 ³ ml/h Q_L : 0-10 ⁵ ml/h	97%		1.7		[99]
Ammonia	Cross T-type square	500 μm ×500 μm $L_c=60$ mm		Q_G : 2.9 × 10 ⁴ ml/h Q_L : 100-300 ml/h	96.45%				[100]
MEA	Cross T-type circular	$d_h=800$ μm , $L_c=25$ mm		Q_G : 0.6-5.4 × 10 ⁵ ml/h Q_L : 0-2400 ml/h	Close to 100%		941.75		[76]
MDEA	Rectangular	1000 μm ×600 μm $L_c=100$ mm		Q_G : 15-90 ml/h Q_L : 20-50 ml/h					[101]
MDEA, MEA	T-type square	400 μm ×400 μm $L_c=36$ mm	Slug, long bubbly	Q_G : 20-160 ml/h Q_L : 20-50 ml/h		8.5×10 ⁻⁴	6		[102]
MEA, DEA, a-MDEA	Circular	$d_h=600$ μm , $L_c=25$ mm		Q_G : 1.8, 3, 3.5 × 10 ⁵ ml/h Q_L : 0.6, 1.2, 1.8 × 10 ³ ml/h	100%, 100% and 82%, respectively				[103]

MEA, DEA, a-MDEA, methanol	Circular	$d_h=800 \mu\text{m}$, $L_c=35 \text{ cm}$		Q_L : 30-270 ml/h	99%		3	[104]
DEA, DEEA	T-type square	$400 \mu\text{m} \times 400 \mu\text{m}$ $L_c=30 \text{ mm}$	Slug, slug annular	Q_G : 10-650 ml/h Q_L : 20-100 ml/h	Close to 100%	33.03×10^{-4}	3.04-20.07	[61]
MEA, DEA	Cross T-type circular	$d_h=800 \mu\text{m}$, $L_c=35 \text{ cm}$		Q_L : 18, 54, 90 ml/h	77.55% and 98.46%		1.91, 3.48	[105]
MEA+DEEA+[Apmim][BF ₄]	T-type square	$400 \mu\text{m} \times 400 \mu\text{m}$ $L_c=30 \text{ mm}$	Taylor-bubbly, Taylor and Taylor-annular	Q_G : 10-650 ml/h Q_L : 20-80 ml/h		22.1×10^{-4}	15	[75]
NaOH	Helical string microchannel	$d_h=500, 1000 \mu\text{m}$		Q_G : 0-13.8 ml/h Q_L : $1-3 \times 10^4 \text{ ml/h}$		2.51×10^{-4}		[106]
Silica nanofluids+SDS	Serpentine rectangular	$800 \mu\text{m} \times 800 \mu\text{m}$ $L_c=120 \text{ mm}$	Taylor	Q_G : 40-700 ml/h Q_L : 40-80 ml/h	80%		6.7	0.59-9.07 [107]
K ₂ CO ₃	T-type square long serpentine	$1000 \mu\text{m} \times 1000 \mu\text{m}$ $L_c=134 \text{ mm}$	Slug, Slug-bubbly	Q_G : 6-600 ml/h Q_L : 60-180 ml/h		6.5×10^{-4}	1.4	[108]
MEA+SDS	T-type square	$400 \mu\text{m} \times 400 \mu\text{m}$ $L_c=30 \text{ mm}$	Slug	Q_G : 20-280 ml/h Q_L : 20-40 ml/h		40×10^{-4}	27	[109]
MEA+DEA/MEA+TEA	Cross T-type, circular	$d_h=600 \mu\text{m}$ $L_c=25 \text{ cm}$	Slug, annular	Q_G : $1.8-9 \times 10^5 \text{ ml/h}$ Q_L : 20-40 ml/h	97.9% and 91.9%			[15]
MEA+[Bmim][BF ₄]	T-type square	$400 \mu\text{m} \times 400 \mu\text{m}$ $L_c=40 \text{ mm}$	Slug flow	U_G : 0.139-0.694 m/s U_L : 0.035-0.087 m/s		20×10^{-4}	12	[94]
L-threonine, L-valine, L-alanine and glycine	T-type square long serpentine	$400 \mu\text{m} \times 400 \mu\text{m}$ $L_c=108 \text{ mm}$	Slug-bubbly	Q_G : 10-120 ml/h Q_L : 10-50 ml/h	Close to 100%		2.5	[95]
HMDA, AEEA, BDA, EG, ChCl	T-type circular	$d_h=2000 \mu\text{m}$ $L_c=5 \text{ cm}$		Q_G : $3.6-9.6 \times 10^3 \text{ ml/h}$ Q_L : 15 ml/h	98%			[110]

3. Effects of operating conditions on the CO₂ absorption in microchannel reactor

The operating conditions have a direct impact on the CO₂ absorption performance of microchannel-based reactors. Therefore, understanding the separate influence of different factors is of great help to promote the overall CO₂ absorption performance.

3.1 Temperature

The operation temperature affects the CO₂ absorption in microchannel in different ways. At high temperature, the reaction rate constant becomes higher, enhancing the mass transfer. Meanwhile, the solution viscosity also decreases, generating thinner liquid film layer in slug/Taylor flow because of the reduced viscous drag[111]. Nevertheless, high temperature can also reduce the CO₂ solubility in the solvent and favor the reverse (desorption) reaction.

Many researches have been performed to reveal the impact of operation temperature. Ye et al.[112] tested the CO₂/MEA system ($C_{CO_2}=11.3$ vol.%; $C_{MEA}=30$ wt.%) in T-junction microchannel reactors (700 $\mu\text{m}\times 300\ \mu\text{m}\times 60$ mm, 700 $\mu\text{m}\times 500\ \mu\text{m}\times 60$ mm, 700 $\mu\text{m}\times 700\ \mu\text{m}\times 60$ mm) under the temperature of 298.15 to 318.15 K. Their results showed the positive effect of temperature rise, i.e., the maximum η_{CO_2} at 318.15 K (95%) is about 5% higher than that at 298.15 K under the same U_G (Fig.4a). Niu et al.[97] tested the CO₂ absorption in PZ activated MDEA in circular channels ($d_h=0.5, 1, 2$ mm, $L_c=180$ mm) under a wider range of temperature (303 K-350 K) and showed that the maximum η_{CO_2} could be reached at 328 K at different U_G (Fig.4b). Aghel et al.[103] compared the η_{CO_2} in three different absorbents (MEA, DEA and a-MDEA) in a circular microchannel ($d_h=600\ \mu\text{m}$, $L_c=25$ cm) at different temperatures (Fig.4c). At low temperature (<300 K), the CO₂ mass transfer flux showed a downward trend due to the dominated physical absorption (especially for a-MDEA). For MEA and DEA, a mass transfer peak due to chemical absorption appeared.

But generally speaking, the influence of operating temperature is relatively small compared to other factors, which will be introduced in the latter sub-sections.

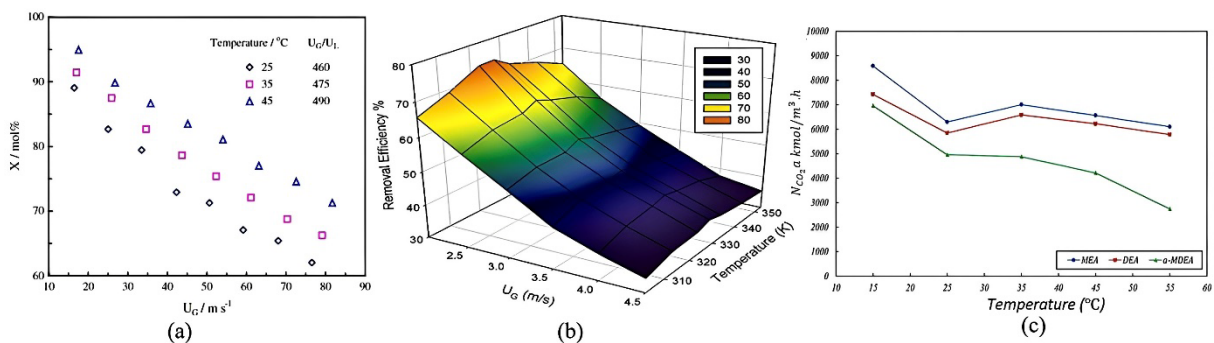


Figure 4 Effect of temperature on the performance of CO₂ absorption in microchannel reactor. (a) CO₂/MEA. Reproduced with permission from Ref.[112], copyright (2013) Elsevier. (b) CO₂/PZ active MDEA. Reprinted with permission from Ref.[97], copyright (2009) American Chemical Society. (c) CO₂/MEA, DEA and MDEA, Reproduced with permission from Ref. [103], copyright (2009) Elsevier.

3.2 Liquid and gas flow rates

The gas and liquid flow rates (velocities) have a significant influence on the performance of CO₂ absorption in microchannel[103,113]. While their ratio (e.g., U_G/U_L) usually determines the two-phase flow pattern as introduced in section 2.1, here their main effect is discussed separately.

At high Q_L , the number of active sites per unit time for accepting and absorbing CO₂ increases, which will improve the $N_{CO_2}a$ and η_{CO_2} . According to the unit cell theory, the global CO₂ absorption performance is largely decided by the amount of chemical absorbent in the unit bubble volume[114]. The increased Q_L would lengthen the liquid slug which also augments the CO₂ mass transfer flux. Kittiampon et al.[100] tested CO₂/ammonia solution system in a T-type microchannel (500 $\mu\text{m}\times 500\ \mu\text{m}\times 60\ \text{mm}$) and showed 10% increase of K_Ga with the increasing Q_L (0.12-0.3 ml/h) (Fig.5a). Aghel et al.[103] verified this trend within a larger Q_L range (0-0.04 L/min) using MEA, DEA or MDEA as the absorbent. Their results showed that the $N_{CO_2}a$ firstly increased rapidly with the increasing Q_L but then reached a plateau (Fig.5b), due to the reduced gas-liquid contact time in the microchannel at high Q_L . Consequently, the Y_{CO_2} might be lowered at excessive Q_L , implying a low utilization rate of the chemical absorbent.

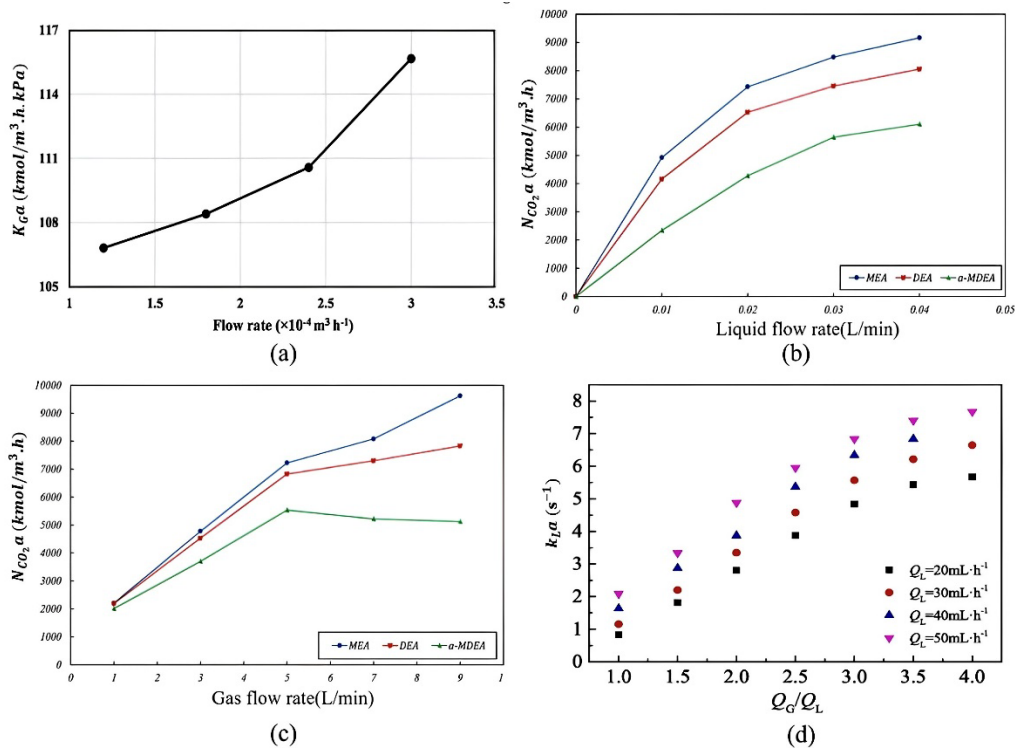


Figure 5 The effect of gas or liquid flow rate on CO₂ absorption performance in microchannel. (a) Effect of Q_L on K_Ga . Reproduced with permission from Ref.[100], copyright (2017) Elsevier. (b) (c) Effect of Q_L on mass transfer flux and effect of Q_G on $N_{CO_2}a$, respectively. Reproduced with permission from Ref. [103],copyright (2019) Elsevier. (d) Effect of Q_G/Q_L on liquid side mass transfer coefficient. Reproduced with permission from Ref.[96], copyright (2019) Elsevier.

3.3 CO₂ partial pressure and system pressure

The influences of CO₂ partial pressure and system pressure have been discussed by several researchers[100,115–117]. High CO₂ partial pressure facilitates the dissolution of CO₂ molecular into the liquid phase. However, the insufficient absorbent molecules for excessive CO₂ involved in the reaction would cause the CO₂ accumulation in liquid phase. Consequently, the driving force for the

mass transfer will be reduced and the dominant liquid side film resistance increased, leading to the decreased mass transfer.

In order to verify this phenomenon, Zeng et al.[117] used the aqueous ammonia as absorbent in a packed column (400 mm in height and 100 mm in diameter) and showed the slight decreasing trend of $K_G a$ with the increase of CO₂ partial pressure (Fig.6a). The negative impact of CO₂ partial pressure increase could be much more pronounced in microchannel reactors. The experimental study of Kittiampon et al.[100] showed 50% decrease of $K_G a$ when CO₂ partial pressure increased from 50 kPa to 300 kPa (Fig.6b).

Meanwhile, high pressure CO₂ is often encountered in some industrial processes such as for the CO₂ removal from high pressure natural gas (2-7 MPa). Yao et al.[115] studied the effect of elevated system pressure (0.1- 4.0 MPa) on the CO₂ absorption by DEA solution in a parallel microchannel reactor. Their results showed clearly the negative impact of high system pressure on the $k_L a$ (Fig.6d). Nevertheless, the results of Niu et al.[97] indicated that the η_{CO_2} increased by 15% to 20% when the system pressure increased from 0.1 to 0.6 MPa (Fig.6c), mainly because of the prolonged reaction time caused by the compressed gas phase. Similar tendency was also reported by Yao et al.[115] with the higher system pressure (up to 4 MPa, Fig.6f). Besides, high system pressure could decrease the energy consumption for the CO₂ absorption process, especially at high Q_L (Fig.6e)[115]. The reasonable control of system pressure can effectively improve the CO₂ absorption performance with a low energy consumption.

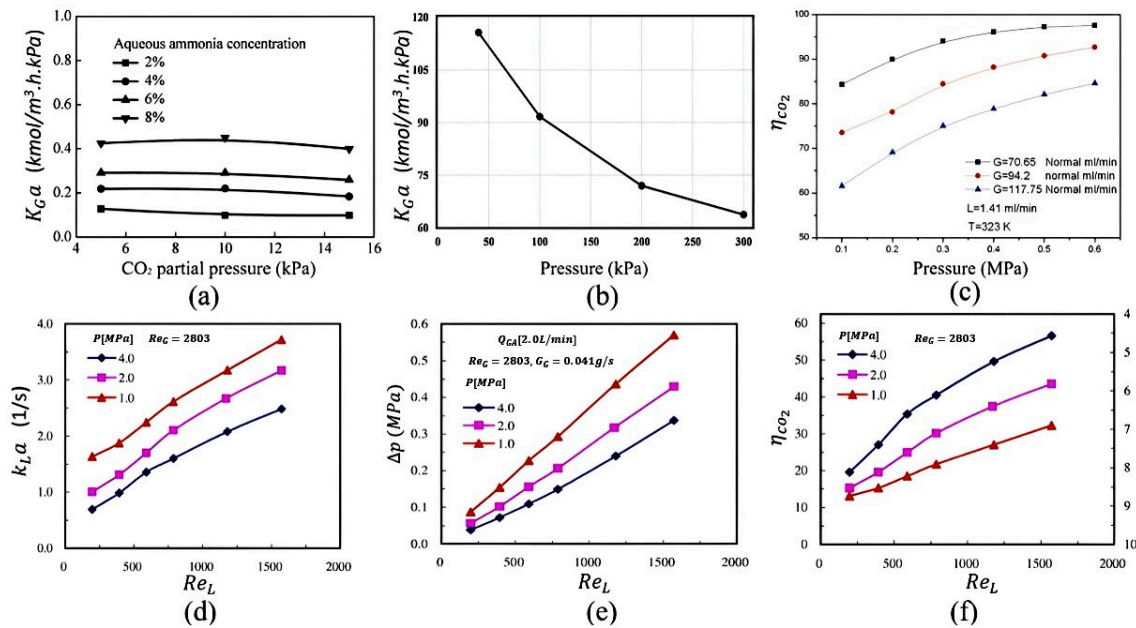


Figure 6 Effect of CO₂ partial pressure and system pressure on the absorption performance. (a) The effect of CO₂ partial pressure on $K_G a$. Reprinted with permission from Ref.[117], copyright (2011) American Chemical Society. (b) The effect of elevated CO₂ partial pressure on the $K_G a$. Reproduced with permission from Ref. [100], copyright (2017) Elsevier. (c) The effect of system pressure on the η_{CO_2} . Reprinted with permission from Ref. [97], copyright (2009) American Chemical Society. (d-f) The effect of elevated system pressure on overall volume mass transfer rate, two-phase pressure drop and η_{CO_2} , respectively. Reproduced with permission from Ref. [115], copyright (2017) Elsevier.

3.4 Absorbent concentration

The absorbent concentration directly influences the CO₂ chemical absorption performance. The study of Aghel et al.[103] clearly showed that increasing the concentration of solvents (MEA, DEA or MDEA)

would greatly augment the $K_G a$ (Fig.7a). Kittiampon et al.[100] showed that in the low concentration range (4-10 wt.%), the $K_G a$ increased monotonously with the increasing concentration of aqueous ammonia (Fig.7b). However, the higher absorbent concentration would augment the liquid viscosity, which may inhibit the CO₂ absorption. Ma et al.[75] found an optimal concentration value (0.6 mol/L) of [Apmim][BF₄] that rendered the highest k_L (20.7×10^{-4} m/s) (Fig.7c). Janati et al.[15] studied the CO₂ absorption using MEA+DEA or MEA+TEA in a T-junction microchannel ($d_h=600 \mu\text{m}$; $L_c=25$ cm). For MEA+DEA solvent, the η_{CO_2} was kept increasing with the increase of both amine concentration and volume percentage. For MEA+TEA solvent, these effects seemed much more sensitive and complicated, showing a parabolic trend, the optimal value being 21.5 wt% and 4 vol/vol%, respectively.

Nevertheless, the ammonia solution at high concentration will cause more serious corrosion problem to the container. For this reason, the concentration of traditional MEA (or most of amine blends) is controlled at ≤ 30 wt% for most of the applications. In the meantime, the development of appropriate high-concentration amine absorbent blends by adding additives is becoming the focus of recent researches. Freeman et al.[118] studied the 8 M PZ in a wetted wall column and found that the $N_{CO_2} a$ could be improved by a factor of 1.5-3.0 compared to 7M MEA. Li et al.[119,120] tested PZ+HMDA and PZ+DAB and showed that the η_{CO_2} could be improved by a factor of 1.5 to 2 compared to 30wt% MEA. Conway et al.[121] tested three types of higher-concentration amine blends (3M MEA+3M DMEA, 3M MEA+3M AMP, and 3M MEA+3M DEEA). The cyclic capacity (re-utilize efficiency of absorbent) could be increased by about 26%-11% compared to 5M MEA absorbent. Other advantages of high-concentration absorbent have also been recognized, such as low thermal degradation rate[122] and low oxidative degradation (4 times slower than 7M MEA)[118].

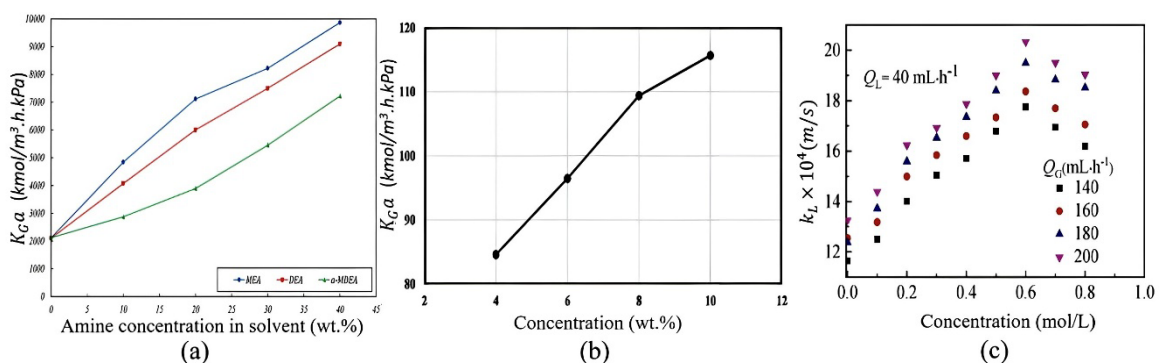


Figure 7. Influence of absorbent concentration on the CO₂ absorption performance. (a) Effect of amine concentration (MEA, DEA and MDEA) on the $K_G a$. Reproduced with permission from Ref. [103], copyright (2019) Elsevier. (b) Effect of aqueous ammonia concentration on $K_G a$. Reproduced with permission from Ref.[100], copyright (2017) Elsevier. (c) Effect of [Apmim][BF₄] concentration on the k_L . Reproduced with permission from Ref.[75], copyright (2021) Elsevier.

3.5 Gas composition

In real carbon capture practice (e.g., power plant flue exhaust decarburization, biogas decarburization, etc.), the CO₂ to be absorbed is not pure but mixed with other gases, its concentration is thereby varied. Nitrogen with stable chemical properties is often used as the carrier gas in current laboratory experiments[100,103], the CO₂ concentration being set at 10 vol.% to simulate most of the practical cases. But for oxygen-enriched combustion of fossil energy, the CO₂ concentration could be much higher. Several studies have been dedicated to evaluate the effect of CO₂ concentration on the absorption performance in microchannel. Akkarawatkhoosith et al.[123] experimentally studied the chemical absorption of CO₂-rich gas (40–60 vol.%) in a T-junction rectangular microchannel (500

$\mu\text{m}\times 500\ \mu\text{m}\times 60\ \text{mm}$) using water as the solvent. It has been shown that the highest η_{CO_2} could reach 70.9% with CO_2 concentration of 53.7%. In another study of microchannel-based biogas decarburization using MEA[124], 65% CH_4 – 35% CO_2 mixture was used to represent the biogas. Results showed 98.9% CH_4 purity and $k_L a$ of $47\text{--}517\ \text{s}^{-1}$, one or two orders of magnitude higher than traditional macroscopic wetted-wall columns (below $10\ \text{s}^{-1}$). Aghel et al.[125] used synthesized gas (60% CH_4 , 40% CO_2) to conduct CO_2 separation and biogas purification in a T-junction microchannel reactor. Their results indicated the augmentation of $K_G a$ by a factor of 5-22 compared with the traditional packed towers.

Other multiple waste gases presenting in the CO_2 absorption process (e.g., SO_2 , NO_2 and other acid gases) can accelerate the degradation of MEA solution, thereby reducing the overall CO_2 absorption performance[126]. For alkaline absorbents, like NaOH, the presence of acid waste gases would also depress the CO_2 absorption because of the low screening capability[127]. At present, CO_2 separation before absorption is still the main method to improve the CO_2 capture performance in various industrial applications.

3.6 Short summary

Aghel et al.[103] have experimentally investigated the contribution rate of different factors on CO_2 absorption performance in the microchannel based reactor. For all three tested absorbents (MEA, DEA and a-MDEA), the influence of temperature is the smallest (Fig.8). For a-MDEA, the absorbent concentration had the largest influence on volumetric mass transfer while for the other two, the liquid-side mass transfer resistance seemed to be the limiting factor. In real practice, such dominant factor should be determined for certain CO_2 absorption solvent and microchannel reactor geometry, so as to better control and improve the CO_2 absorption performance.

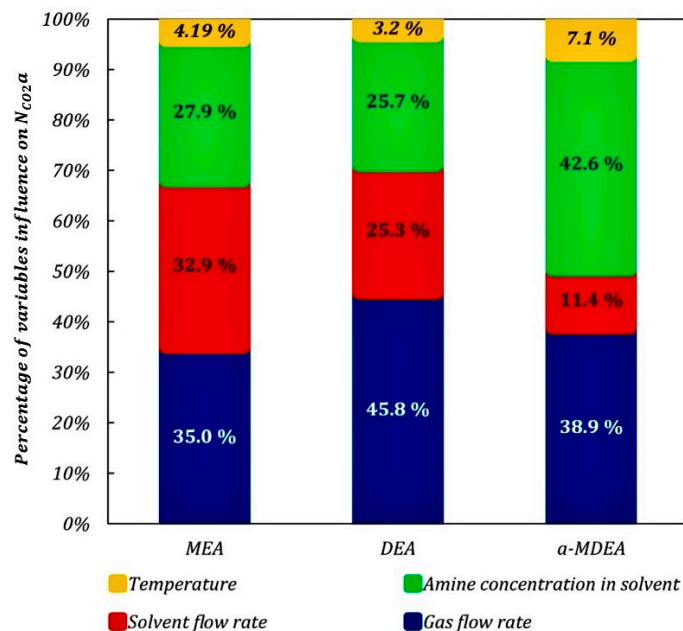


Figure 8 Sensitivity analysis for the effect of operating variables on the mass transfer flux. Reproduced with permission from Ref.[103], copyright (2019) Elsevier.

4. Interfacial & local parameters of CO₂ absorption in microchannel

Gas-liquid interfacial and local parameters are essential for the comprehensive understanding of the transport process, allowing the development of the mass transfer theory/model on one hand, and the performance optimization of the CO₂ absorption device on the other hand. In this section, the identification and characterization of such interfacial & local parameters in microchannel are presented. While the CFD simulation methods are frequently employed for this purpose, special focus is given on the experimental measuring techniques.

4.1 Liquid film thickness (LFT)

The LFT around the Taylor bubbles is in close relation to the mass transfer of gas-liquid two-phase flow in microchannel[128–131]. The mass transfer rate usually decreases with the increase of LFT due to the larger liquid-side mass transfer resistance[132] (Fig.9a).

Many studies have been devoted to the precise measurement of LFT and the development of empirical correlations based on some dimensionless numbers (Re , Ca , We or others), as summarized in Table 4. For example, Han & Shikazono[133] used laser focus displacement meter (LFDM) to measure the LFT at small Ca number condition (Fig.10c). Two semi-empirical correlations were put forward to predict the LFT under bubble steady motion and acceleration motion, respectively (cf. Table 4). By using the laser induced fluorescence (LIF) method, Bartkus & Kuznetsov[134] showed the deviation of the measured LFT from the Taylor LFT prediction model especially for the position away from the microchannel corner (Fig.10b). Cheng et al.[135] used the nano-particle tracking velocimetry technique (Mn-PTV) to measure the local oscillation of bubble LFT in square microchannels. Polystyrene fluorescent nanoparticles (20 nm) were used as the tracer particles and the measuring uncertainty was estimated to be smaller than 8%. Their result showed that the LFT exhibited periodic changes and with the decrease of channel dimension, the lag time of bubble movement was significantly shortened (Fig.10d).

It should be noted that most of the experiments and the proposed correlations do not consider the influence of mass transfer. Experiments and simulation studies combining the CO₂ mass transfer and dimensionless LFT are especially needed for a better understanding of CO₂ absorption in microchannel.

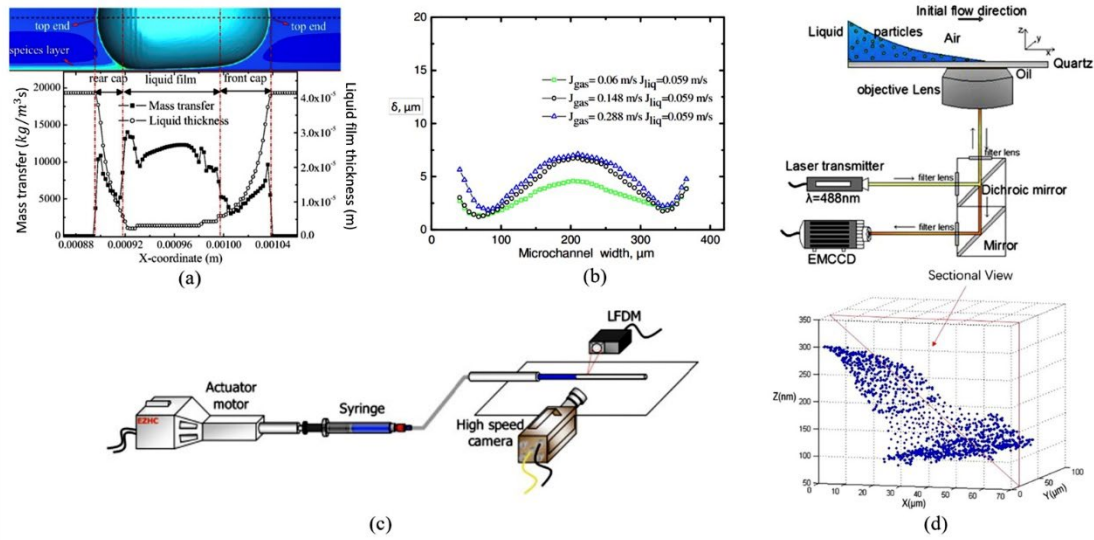


Figure 9 Investigation of LFT distribution around the gas-liquid interface in microchannel. (a) LFT vs. mass transfer performance of the Taylor bubbly flow on different position obtained from 3D simulation. Reproduced with permission from Ref.[132], copyright (2016) Elsevier. (b) LFT distribution along the microchannel width measured by LIF method. Reproduced with permission from Ref. [134], copyright (2016) EDP Sciences. (c) LFT distribution around the bubble acceleration mode measured by LFD. Reproduced with permission from Ref. [133], copyright (2010) Elsevier. (d) LFT distribution around the oscillation bubble using the Mn-PTV method. Reproduced with permission from Ref. [135], copyright (2020) Elsevier.

Table 4 Summary of main researches about the measurement of dimensionless liquid film thickness δ_0/d_h for gas-liquid two phase flow in microchannel.

Microchannel/capillary parameters	Fluids	Flow pattern/status	Investigation method and details	Semi/empirical formula for LFT prediction	Ref.
Glass tube: $d_h=2.26$ mm	Air Water	Single slug	Bubble-tube measurement	$\frac{\delta_0}{d_h} = 0.5(Ca)^{0.5}$	[136]
Glass tube: $d_h=2; 3$ mm	Air Water	Taylor	Visual measurement	$\frac{\delta_0}{d_h} = \frac{0.67Ca^{2/3}}{1 + 3.35Ca^{2/3}}$	[137]
Capillary tubes $1 \text{ mm} < d_h < 2 \text{ mm}$	-	Taylor	Finite-difference simulation	$\frac{\delta_0}{d_h} = 0.36(1 - e^{-3.08Ca^{0.54}})$	[138]
Capillary tubes $d_h=0.84; 1.24; 1.56, 2.92$ mm	Air Silicone oils; ethanol; alkanes	Single slug	Visual camera shooting (Capture frequency: 50 fps)	$\frac{\delta_0}{d_h} = \frac{1.34Ca^{2/3}}{1 + 3.35Ca^{2/3}}$	[139]
Square channel $1.56 \text{ mm} \times 1.56 \text{ mm}$	Air Water	Taylor	Small platinum micro-probes method (Sample frequency up to 10 000 Hz)	$\frac{\delta_0}{d_h} = 0.72(1 - 0.7e^{-2.25Ca^{0.445}})$	[140]
Circular tubes $d_h=0.5; 0.7$ and 1.0 mm	FC-40; Air Ethanol; water	Liquid-gas interface	LFDM Precision 99% (Resolution: $0.01 \mu\text{m}$; Response time: $640 \mu\text{s}$) Interferometer (Capture frequency: 5000 fps; Uncertainty: $0.534 \mu\text{m}$)	$\left(\frac{\delta_0}{d_h}\right)_{steady} = \frac{0.67Ca^{2/3}}{3.13Ca^{2/3} + 1 + 0.504Ca^{0.672}Re^{0.580} - 0.352We^{0.629}}$	[133]
Parallel channels: $h=0.1; 0.3; 0.5$ mm	Air Ethanol	Liquid-gas interface	LFDM (Capture frequency: 1000 fps; Precision: 99%; Resolution: $0.01 \mu\text{m}$)	$\frac{\delta_0}{d_h} = \frac{0.67Ca^{2/3}}{3.13Ca^{2/3} + 1 + 0.504Ca^{0.672}Re^{0.589} - 0.352We^{0.629}}$ ($Re < Re$ critical)	[141]
Circular tube $0 < Ca < 1.9$	-	Horizontal	Bretherton model based numerical analysis	$\frac{\delta_0}{d_h} = \frac{1.38Ca^{2/3}}{1 + 3.732Ca^{2/3}}$	[142]
Circular tubes $d_h=1$ mm	FC-40; air Ethanol; water	Slug Taylor	LFDM (Precision 99%; Resolution $0.01 \mu\text{m}$; Response time $640 \mu\text{s}$)	$\left(\frac{\delta_0}{d_h}\right)_{accel} = \frac{0.968Ca^{2/3}}{Bo^{0.414} + 4.838Ca^{2/3}}$	[143]

Rectangular microchannel 420 μm ×280 μm , 720 μm ×1500 μm	Nitrogen Water	Elongated bubble	LIF (Resolution: 0.5 μm)	-	[134]
Circular tubes: $d_h=0.7$; 1.0 and 1.3 mm	FC-40 Water; ethanol	Taylor-bubbly	Interferometer and LFDM (Precision: 99%; Resolution 0.01 μm)	$\left(\frac{\delta_0}{d_h}\right)_{decel}$ $= \frac{0.67Ca^{2/3}}{3.36Ca^{2/3} - 0.352We^{0.640} + (1 + 0.534Ca^{0.672}Re^{0.593})(e^{-0.02Bo_{decel}^{1.45}})}$	[144]
T-type rectangular microchannel 100 μm ×83 μm	CO ₂ Ethanol; methanol	Taylor-bubbly	Volume of Fluid (VOF) based 3-D simulation	-	[132]
Circular tube $d_h=0.305$; 0.715 and 1.305 mm	FC-40; air Water; ethanol	Bubbly	Arbitrary-Lagrangian– Eulerian based simulation	$\frac{\delta_0}{d_h} = \frac{1.34Ca^{2/3}}{3.13Ca^{2/3} + 1 + 0.504Ca^{0.672}Re^{0.589} - 0.305We^{0.664}}$	[145]
Square microchannel $d_h=510$; 1020 μm	Air Water	Slug	High-speed camera visualization (Precision: >93.2%; Resolution: 2.8 μm)	$\frac{\delta_0}{d_h} = 0.085Ca^{-0.137}$ (For corner film thickness)	[146]
Rectangular microchannel 3 mm×3 mm; 1.6 mm×1.6 mm; 0.5 mm×0.5 mm and 0.3 mm×0.3 mm	Air Water	Liquid-gas interface	Mn-PTV (Uncertainty < 8%; Resolution 0.02 μm ; Capture frequency 500 fps)	-	[135]

4.2 CO₂ local concentration

The chemical reaction proceeds directionally according to the CO₂ concentration gradient in the liquid, the mass transfer rate being non-uniform in different positions in microchannel. Knowing the local CO₂ concentration distribution between the bubble border and the liquid slug is thereby much needed.

CFD simulation has been frequently used[147–149]. Soh et al.[147] studied the diffusion and the distribution of CO₂ molecules for a bubble moving in the silicone oil in a microchannel using the VOF model (Fig.10a). Li et al.[150] successfully simulated the CO₂ absorption in a tube-in-tube microchannel (Fig.10b), using the modified eddy-cell model coupled with VOF method. Dong et al.[151] simulated the CO₂ absorption by water, ethanol solution, 0.2 M MEA solution, and 0.2 M NaOH solution in a circular microchannel ($d_h=500\ \mu\text{m}$) using the initial unit model. The CO₂ distribution in liquid phase around the bubble in CO₂-water and CO₂-NaOH system at the same reaction time were compared (Fig.10d), demonstrating the dominant role of chemical reaction on quick CO₂ mass transfer.

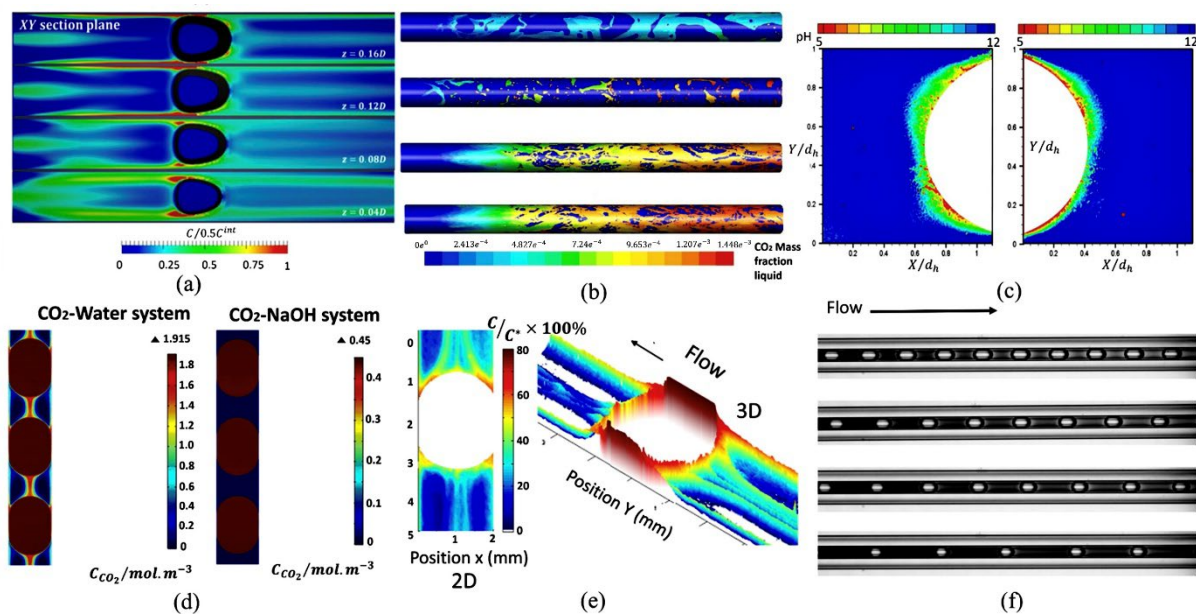


Figure 10 Investigation of concentration distribution of gas-liquid two-phase flow in microchannel. (a) Dissolved CO₂ molecules distribution in silicone oil by CFD simulation. Reproduced with permission from Ref. [147], copyright (2017) Springer. (b) Simulation result of CO₂ mass fraction distribution in a microporous tube-in-tube microchannel. Reproduced with permission from Ref. [150], copyright (2020) Elsevier. (c) CO₂ concentration distribution in liquid phase around bubbles detected by pH-Sensitive LIF method. Reprinted with permission from Ref. [152], copyright (2012) American Chemical Society. (d) CO₂ concentration in the liquid phase around the bubble (CO₂-H₂O and CO₂-NaOH system). Reproduced with permission from Ref. [151], copyright (2020) Wiley. (e) 2D and 3D simulation of gas molecules diffusion in the liquid phase around a moving bubble in microchannel. Reproduced with permission from Ref. [153], copyright (2013) Elsevier. (f) CO₂ concentration distribution in water measured by pH sensitive colorimetric method. Reproduced with permission from Ref. [154], copyright (2022) Elsevier.

Regarding experimental techniques, Deleau et al.[78] used Raman spectroscopy and showed that the local CO₂ concentration along the capillary tube presented an upward trend but accompanied with a reduced growth rate. More recently, Deleau et al.[154] further explored the CO₂-water segment flow mass transfer performance in a straight circular microchannel ($d_h=250\ \mu\text{m}$) under high pressure (10 MPa) by using pH sensitive colorimetric method. Their results showed that the $k_L a$ ranged from 1 to 13 s⁻¹ along the length direction (Fig.10f). Kuhn & Jensen[152] developed a pH-sensitive LIF method (5-(and-6)-carboxy SNARF-1 used as fluorescent dye) and showed that the mass transfer happened mainly at bubble caps in microchannel (Fig.10c). Nevertheless, only the CO₂ concentration distribution of a 2D

plane could be obtained, due to the limitation of excitation chip laser. Ichiyanagi et al.[155] implemented the ‘confocal micro-PIV +LIF’ method to investigate the CO₂ concentration distribution in spiral and meandering microchannels (400 μm×400 μm), illustrating clearly the dominating mass transfer at the bubble caps. Dietrich et al.[153] studied the oxygen-water mass transfer process in a straight circular microchannel ($d_h=750\ \mu\text{m}$) using oxygen-sensitive dye and a monochromatic CCD high-speed camera (Fig.10e). This colorimetric technique could be a promising tool for local CO₂ concentration measurement in microchannel.

4.3 Local liquid velocity

Various approaches have been employed to capture the liquid velocity field of Taylor/bubbly flow in microchannel (especially near the gas-liquid interface), most of them demonstrating the existence of symmetrical[151,156] or asymmetrical[114] local fluid microcirculations in the liquid slug. By using the VOF model, Yang et al.[148] simulated the air/water slug flow in a straight circular microchannel ($d_h=200\ \mu\text{m}$). Validated hydrodynamics coupled with chemical reaction pushed mass transfer term was used as solver to capture the circulatory patterns in the segment flow (Fig.11a). Dong et al.[151] showed the symmetrical liquid velocity profile between two CO₂ bubbles around a water slug in a microchannel ($d_h=500\ \mu\text{m}$) by using the unit bubble model and neglecting the gravity effect and the bubble volume change (Fig.11b). Yin et al.[57] also used the VOF model to simulate the liquid velocity field of CO₂-MEA/[Bmim][BF₄] aqueous in a microchannel (400 μm×800 μm×30.4 mm), showing the strongly perturbed velocity profiles due to interior micro-baffle structures (Fig.11c). Similar phenomenon has also been reported for concave heart-shaped groove microchannel (Fig.11d)[157].

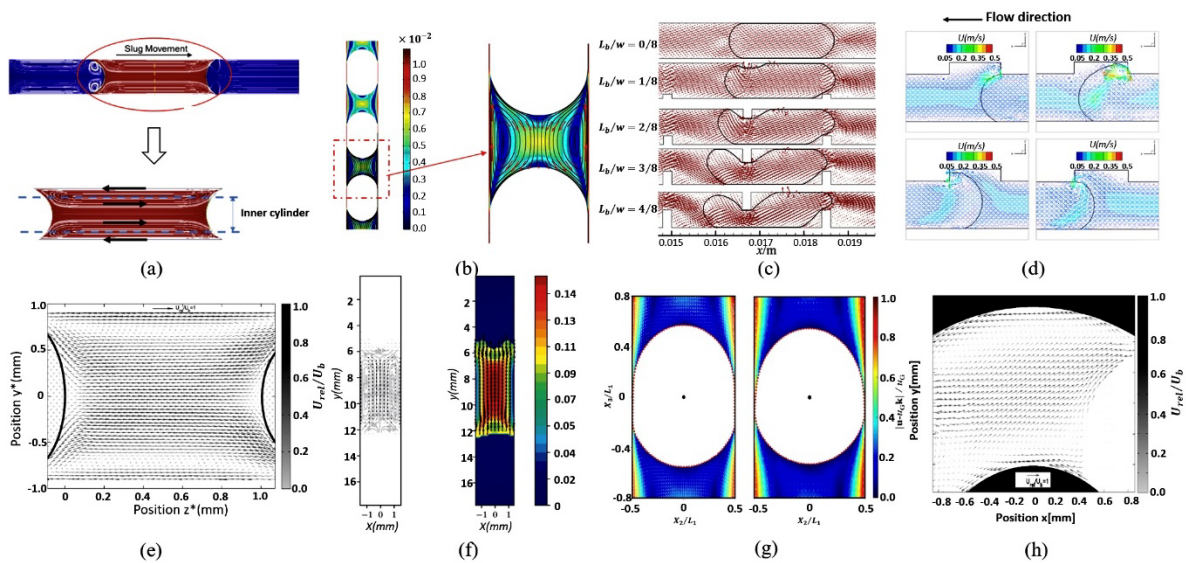


Figure 11 Flow velocity field around Taylor bubbles in microchannel. (a) Circulatory patterns in the segment flow by VOF model. Reproduced with permission from Ref. [148], copyright (2017) Elsevier. (b) Simulated velocity and streamline distribution in the micro channel for the CO₂-water system. Reproduced with permission from Ref. [151], copyright (2020) Wiley. (c) Liquid velocity distribution around the bubble in baffled microchannel by the VOF method. Reproduced with permission from Ref. [57], copyright (2019) Elsevier. (d) Liquid velocity distribution in groove etched microchannel by the VOF method. Reproduced with permission from Ref. [157], copyright (2021) Elsevier. (e)(h) Symmetrical relative velocity field in the liquid slug between two Taylor bubbles in straight channel (flow direction: left to right) and asymmetrical relative velocity field in the liquid slug between two Taylor bubbles in a meandering channel (flow direction: left to right) captured by micro-PIV method, respectively. Adapt with permission from Ref. [114], copyright (2012) Elsevier. (f) Experimental PIV time-averaged velocity fields for slug liquid between two bubbles. Reproduced with permission from Ref. [156], copyright (2018) Elsevier. (g) Liquid velocity vectors around a bubble measured by PTV technique. Reproduced with permission from Ref. [161], copyright (2021) Elsevier

Experimentally, Zaloha et al.[114] used micro PIV method and showed that the liquid microcirculation rate gradually increased with the shorter liquid slug at higher U_G and U_L (Fig.11e). Butler et al.[156] used both the PIV and PLIF-I techniques to investigate the O₂-water mass transfer process in a circular channel ($d_h=3$ mm). Both the velocity and O₂ concentration fields were measured, showing great consistency with each other (Fig.11f). Recently, the PTV method has also been applied to measure the velocity field[158–160]. Azadi & Nobes[161] explored the liquid flow velocity around a slug bubble, especially in the thin film and at the corners, in a square mini-channel (3 mm×3 mm) (Fig.11g). Particularly for meandering microchannel, some researchers reported the velocity asymmetry and micro-circulations in the bend position (Fig.11h), implying a possible way to enhance the mass transfer using this geometry[114]. This point will be further discussed in the next section of the paper.

5. Intensification measures for CO₂ chemical absorption in microchannel reactors

The application of microchannel-based reactors for CO₂ chemical absorption can greatly reduce the size of the equipment, but some limitations still exist such as the lowered throughput and the higher energy consumption to overcome the pressure drop. Further intensifying this process is still the focus of researches, as classified and reviewed in this section. Detailed information about these studies may be found in Table 5.

5.1 Setting the global microchannel geometry

Instead of the common straight channel, serpentine and spiral shapes are proposed and used to strengthen the CO₂ absorption and to save the space in the length direction for easier stacking. These curved channel geometries are expected to disturb the moving boundaries of bubbles (interfaces) by the dean vortex effect[162,163], thereby promoting the mass transfer. Yang et al.[164,165] showed the significantly increased mass transfer rate owing to the enhanced liquid mixing in a curved microchannel (Fig.12a). Zhou et al.[40] designed and experimentally tested a serpentine rectangular microchannel (600 μm ×600 μm) for CO₂ absorption by MEA (Taylor-bubbly flow, Fig.12b), showing 40% increase of the $K_G a$ compared to that of straight channel. Similar improvement effect has also been reported by Yao et al.[166]. Seo et al.[167] investigated the chemical CO₂ absorption by nickel nanoparticles (NiNPs) catalyzed MEA absorbent in a serpentine microchannel (Fig.12c). Their results showed that compared to the straight channel, the average CO₂ absorption rate could be improved by 34% with the single effect of NiNPs catalyst, and by 54% with the combined effect of catalyst and serpentine geometry. Tan et al.[168] reported that the k_L of CO₂/N₂-NaOH solution segmented flow could be doubled (2.7×10^{-4} m/s) in a curve-shaped microchannel compared to that in the straight channel (1.3×10^{-4} m/s). Higher k_L could be achieved by decreasing the radius of the U-turns because of the strengthened gas-liquid disturbance.

Kuhn & Jensen[152] compared the $k_L a$ of CO₂/alkaline solution between a spiral and a meandering microchannel reactor (Fig.12d) and found that the spiral geometry performed much better owing to the decreased residence time and increased gas volume transport fraction. MacInnes et al.[169] tested

a spiral minichannel rotating reactor (1.5 mm×4 mm) for CO₂/N₂ absorption by MEA solution, the $\eta_{CO_2} > 90\%$ could be reached. Pang et al.[108] experimentally investigated the CO₂ absorption in potassium carbonate solution using a serpentine microchannel (1 mm×1 mm) with 6 elbows. Their results indicated much higher k_L (0.5-2.5×10⁻⁴ m/s) than that of straight microchannel (0.07-13×10⁻⁵ m/s)[170] and the maximum pressure drop was smaller than 3.49 kPa. All these researches have demonstrated that setting the global microchannel geometry is an effective and practical way for the design of microchannel-based CO₂ absorbers.

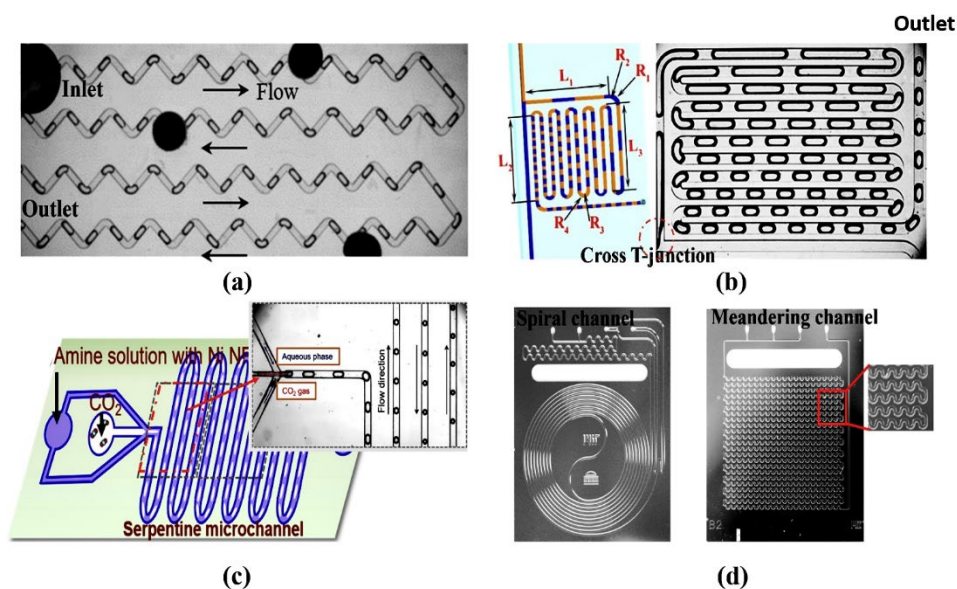


Figure 11 Setting of global microchannel geometry to enhance the CO₂ absorption performance. (a) Continuous 90° meandering microchannel. Reproduced with permission from Ref. [165], copyright (2017) Elsevier. (b) Serpentine microchannel with T-type junction. Reprinted with permission from Ref. [40], copyright (2020) American Chemical Society. (c) Serpentine microchannel with hedge-type mixing structure. Adapted with permission from Ref. [167], copyright (2020) Elsevier. (d) Spiral- (left) and meandering- (right) microchannel reactor used for the CO₂/alkaline solution two-phase flow experiments study. Reprinted with permission from Ref. [152], copyright (2021) American Chemical Society.

5.2 Structuration of channel walls

The structuration of channel walls by installing flow disturbance elements (micro grooves[35,66,171], micro protrusion obstacle[57,172], sudden expansion/shrink, etc.) could induce the local eddy flow of liquid phase and deform the gas-liquid interface, both effects enhance the mass transfer. Chen et al.[35] tested a straight microchannel (800 μm×400 μm×35.2 mm) etched with heart-shaped grooves (Fig.13a) and found that the $k_L a$ for CO₂-[Bmim][BF₄] aqueous solution could be increased by 150%-210% compared with the smooth microchannel. Similar enhancement rate for CO₂-NaOH solution has been reported by Cantu-Perez et al.[66] owing to the grooves (100 μm) etched in a falling film microreactor constituting of 16 parallel rectangular mini-channels (1200 μm×400 μm×66.4 mm) (Fig.13b).

For micro protrusion obstacle, the most commonly used structures include rectangular, triangular and cylindrical shapes having different flow disturbing capacities[173]. Among them, the rectangular protrusion obstacle has been reported to be the most effective for single-phase flow in microchannel[174], thereby also frequently applied for gas-liquid flows. Yin et al.[175] fabricated a rectangular microchannel (400 μm×800 μm) with staggered rectangular obstacles (Fig.13c) and investigated the effect of geometrical parameters (length, arrangement, etc.) on the CO₂/water mass

transfer performance. Their results showed that the maximum $k_L a$ could be increased by a factor of 2.8 owing to the greatly shredded liquid-gas boundary layer by obstacle elements.

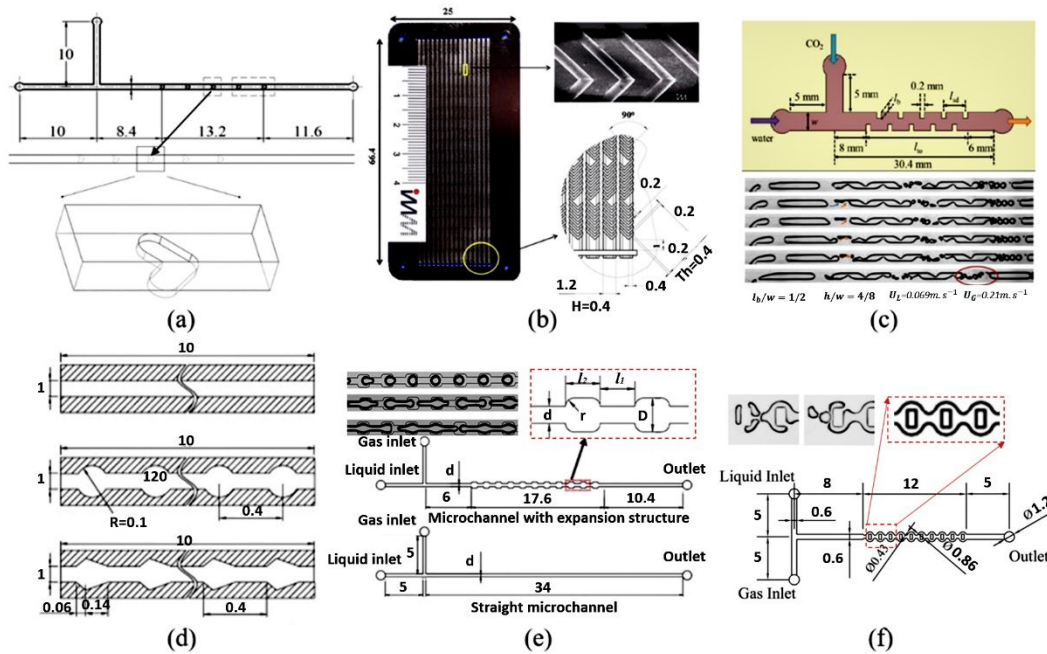


Figure 13 Wall structuration for microchannel gas-liquid reactors. (a) Straight microchannel etched with heart-shaped grooves. Reproduced with permission from Ref. [35], copyright (2021) Elsevier. (b) Parallel mini-channels reactor with rectangular grooves. Reproduced with permission from Ref. [66], copyright (2012) Elsevier. (c) Microchannel with protrusion baffle structure. Reproduced with permission from Ref. [175], copyright (2020) Elsevier. (d) Microchannel accompanied with fan and triangular shaped sudden expansion structure. Reproduced with permission from Ref. [176], copyright (2015) Elsevier. (e) Microchannel accompanied with arced rectangular shape sudden expansions structure. Reproduced with permission from Ref. [59], copyright (2021) Elsevier. (f) Combined sudden expansion structure with rectangular obstacle in the middle. Reproduced with permission from Ref. [58], copyright (2022) Elsevier.

Some researchers have demonstrated that sudden expansion/ shrink structured microchannel (Fig. 13d) has the unique advantage in inducing two-phase mixing, i.e., the oscillation of gas bubble and surrounding liquid[176–178]. Zhang et al.[59] fabricated the arced sudden expansion structured microchannel reactor to test the CO₂ absorption performance in [Bmim][BF₄] aqueous solution. Shrink and expand slug flow was captured (Fig.13e), leading to an improvement of $k_L a$ by a factor of 1.2-2.4 compared with the smooth microchannel with a total pressure drop smaller than 5 kPa. Adding micro-obstacles in the middle of the microchannel has also been proposed to generate the bubble breakup. Yin et al.[58] combined the sudden expansions layout with rectangular obstacle (600 μm ×300 μm) and observed complete and partial bubble breakups (Fig.13f). The $k_L a$ could be augmented by a factor of 2.74 with the maximum pressure drop smaller than 12 kPa, acceptable for most of the industrial applications[179]. Further design and shape/topology optimization of the obstacle geometry for the microchannel for intensified mass transfer process with reasonable pressure drop could be an interesting topic for future researches.

5.3 Special operating modes

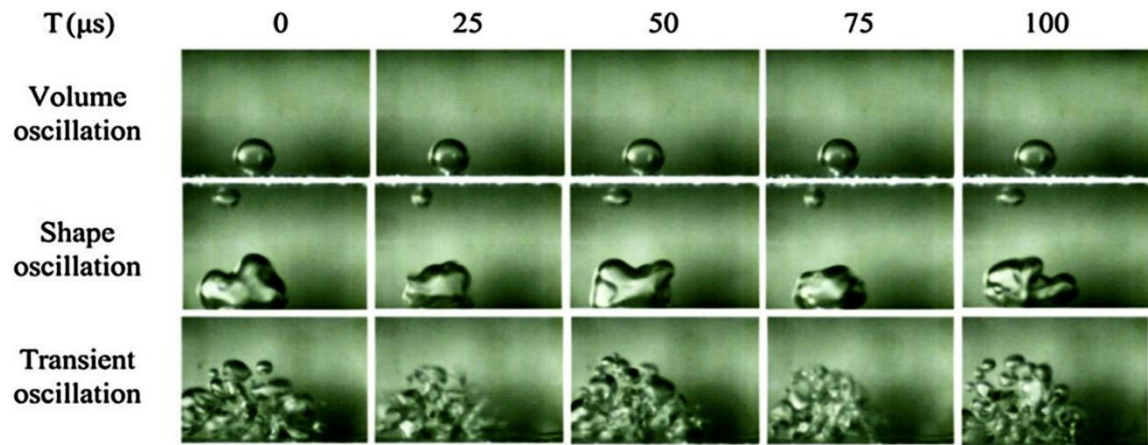
Applying external operating conditions has also been considered, including ultrasound[41,180], electric field[172,181], and special working modes such as high system pressure[115] or mechanical oscillating.

The ultrasound imposed on two-phase flow could induce the regular oscillation of both bubbles (volume oscillation, shape oscillation and high frequency transient oscillation[182], Fig.14a) and liquid slugs in the microchannel, drastically increasing the gas-liquid interfacial area and creating more local vortices and liquid streaming near the two-phase interface[183,184]. Dong et al.[41,184] used high-power ultrasonic (100 W; 20 kHz) to intensify the CO₂-DI water slug flow mass transfer in a serpentine minichannel (1 mm×1 mm). Their results demonstrated that the $k_L a$ could be enhanced by a factor of 3.3–5.7 with the increase of ultrasonic power from 0 to 70 W. Akbari et al.[185] employed the 1.7 MHz ultrasound waves generated by piezoelectric transducer to accelerate the CO₂ absorption by NaOH solution (Fig.14c), leading to the increased $k_L a$ and a by 21% and 22%, respectively. Among different two-phase flow patterns, the bubbly flow has shown to be the most sensitive to ultrasound waves thus has the most significant enhancement by oscillatory effect. Zhang et al.[186] investigated the effect of ultrasonic wave frequency (20, 28, 40 kHz) and surfactant (sodium dodecyl sulfate) on CO₂ absorption performance in rectangular channels (0.5-2.0 mm in width). The determined optimum condition was at low frequency (20 kHz), high acoustic power (0.14 W/mL) and high surfactant concentration (Fig.14d), resulting in the enhancement of $k_L a$ by a factor of 3 to 22.

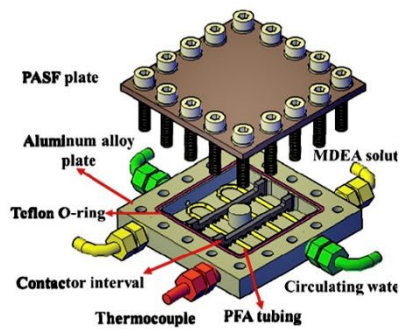
The external electric field has been used for osmotic flow to enhance the liquid mixing in the microchannel[172]. Hoseini et al.[187] investigated the effect of external electric field (133, 200, or 266 kV/m) on CO₂ absorption by water/Fe₃O₄ solution in a small channel ($d_h=6$ mm). 16% increase of k_L could be achieved with 266 kV/m electric field.

Lliuta & Larachi[188] explored the effect of mechanical oscillation (rotation, up-down and rocking oscillation) on CO₂ absorption in MEA solution in packed-bed columns (Fig.14e). The heaving motion (up-down) has shown to result in the best CO₂ absorption performance. Such external oscillatory operation could be inspiring for microchannel-based CO₂ absorption devices.

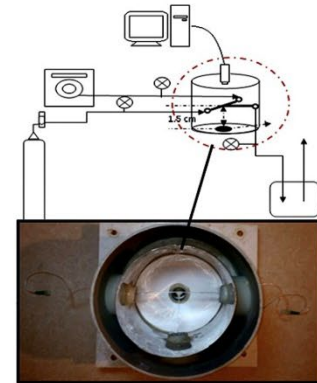
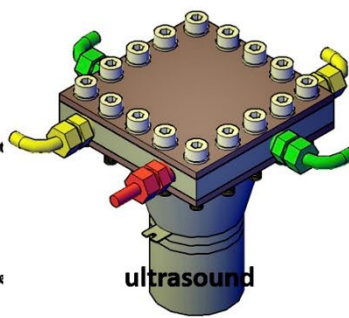
While the above-mentioned methods show great potential on improving the CO₂ absorption performance, they are rarely applied to real industrial cases due to the additional power input and high equipment investment. For example, the power input for conventional ultrasonic chemical reactor is about 0.05-0.6 W/mL[189–191], meaning that at least 50 KW of additional input power is required for unit volume (1 m³) of absorption liquid[184] which is hardly affordable in real industry applications.



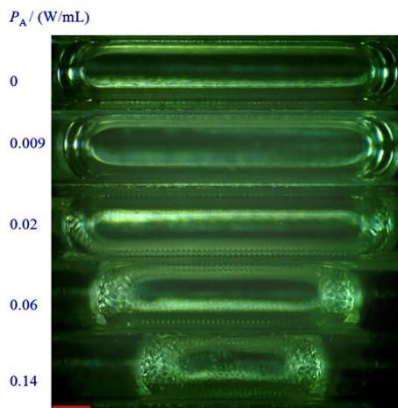
(a)



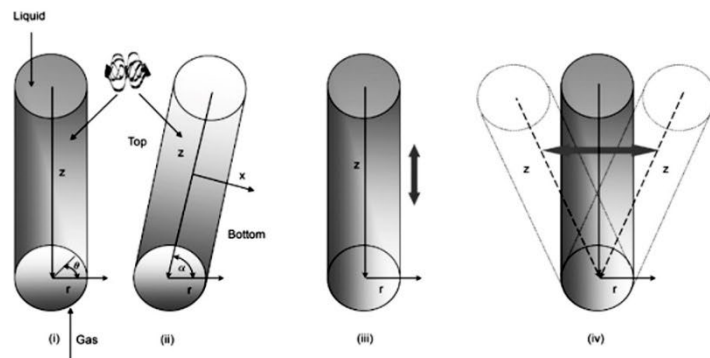
(b)



(c)



(d)



Rotational oscillation

Up and down oscillation

Rocking oscillation

(e)

Figure 14 Special operating modes for intensifying the CO_2 chemical absorption performance. (a) Oscillations caused by different ultrasound frequency. Reproduced with permission from Ref. [182], copyright (2020) Elsevier. (b) High-power ultrasonic accompanied serpentine mini-channel to strengthen the CO_2 absorption. Adapted with permission from Ref. [180], copyright (2019) American Chemical Society. (c) Ultrasound accompanied T-junction microchannel CO_2 absorption system. Reproduced with permission from Ref. [185], copyright (2017) Elsevier. (d) Oscillation of bubble surface under different acoustic power. Reproduced with permission from Ref. [186], copyright (2021) Elsevier. (e) Schematic of mechanical oscillation mode. Adapted with permission from Ref. [188], copyright (2018) Elsevier.

5.4 Integration of microchannels

The microchannel integration involves the use of a multitude of channels instead of single microchannel in the device, which is considered as an essential step for the scaling-up for industry-level application. If properly conceived and controlled, the integration of microchannels is equivalent to repeating settings for a single microchannel with high CO₂ absorption performance, but greatly increased throughput (amount of CO₂ processed per unit time). Based on the basic type of straight microchannel, the most commonly used integration pattern at present is through the parallelization (numbering-up), and the problem of connection has been particularly addressed. Tree-like arborescent structure has been frequently utilized to equally distribute and collect the fluids[192,193]. For example, Yue et al.[194] investigated the CO₂-water mass transfer performance in a 16 parallel microchannel contactor equipped with dichotomic-tree gas and liquid distributors (Fig.15b). It has been observed that the multi-channel concept could be beneficial for maintaining the slug flow pattern at high Q_G but disordered two-phase flow pattern would lead to the deterioration of mass transfer performance. Yao et al.[115] fabricated a tree-like reactor (Fig.15c) with 16 main rectangular microchannels (300 μm ×600 μm) and 8 sub microchannels (300 μm ×800 μm) to perform the CO₂ absorption in DEA solution under elevated system pressures (4 MPa). The $k_L a$ ranging from 1.59 to 90 s⁻¹ could be obtained mainly due to the increased contacting (residence) time of two-phase flow in the reactor. Zhu et al.[195] designed 4-parallel channel microreactor to carry out the CO₂ absorption (Fig.15a) and showed that the average $k_L a$ of the multi-channel collection was 0.3-3.5 s⁻¹, 5%-10% lower than single microchannel. However, the two-phase flow fluctuation caused by the increase of Q_L and Q_G could be eliminated.

Mesh collection is another way to integrate the microchannels[196,197]. Constantinou & Gavriilidis[198] tested and compared the CO₂ absorption performance in 2M NaOH solution by three mesh-structured reactors (pore size: circle 25 μm in diameter; rectangular 25 μm ×75 μm ; and square 35 μm ×35 μm , 100 μm in thickness) (Fig.15d). The increased two phase contact area due to mesh structure would not only help stabilize the gas/liquid interface but also augment the CO₂ absorption performance. Reducing the pore size (5-25 μm) and increasing the open area could furtherly increase the η_{CO_2} by 20%-25% compared to the previous reactor (Fig.15e)[199].

Some researchers also put forward the structure integration with nature-inspired geometries. For example, Zhang et al.[200] designed a honeycomb-like fractal type reactor ($d_h=3$ mm) to investigate the CO₂- MEA absorption performance (Fig.15f). Compared to a serpentine tubular reactor, both the η_{CO_2} and the CO₂ absorption rate could be increased by about 30%. Recently, the use of triply periodic minimal surface (TPMS) geometries as the CO₂ absorber has been reported owing to its higher a and smooth surface[201,202], offering an interesting potential for the design of macro-sized CO₂ absorbers. For example, Singh et al.[201] designed a Schwarz-D cell based CO₂ absorber (Fig.15g) consisting of two separated domains, one for CO₂ and absorbent mixed flow and the other for the cooling fluid for reaction heat management. Sithamparam et al.[203] numerically studied the gyroid-based CO₂ absorber (Fig.15h) and showed 10% increase of η_{CO_2} compared with the flat-sheet membrane absorber. Despite that this absorber design relies on membrane permeation, it shows a great potential for the development of macro-sized CO₂ absorbers with high efficiency.

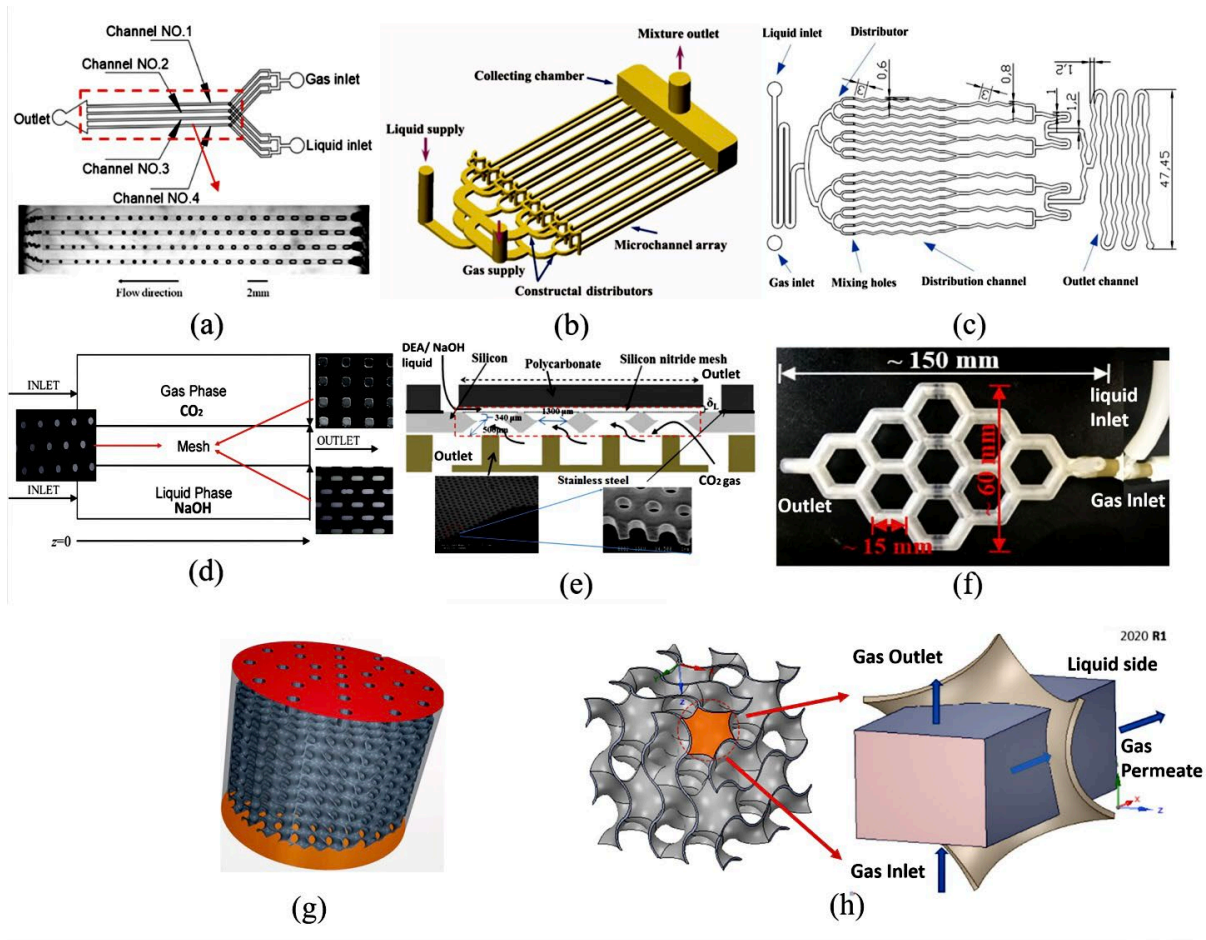


Figure 15 Different types of microchannel integration for CO₂ chemical absorption. (a) 4-parallel microchannel-based CO₂ absorption reactor with tree-like distributor. Reproduced with permission from Ref. [195], copyright (2020) Elsevier. (b) 16-parallel microchannel CO₂ absorber with dichotomic tree-like gas and liquid inlet distributors. Reproduced with permission from Ref. [194], copyright (2010) Wiley. (c) Tree-like microchannel based CO₂ absorption device. Reproduced with permission from Ref. [115], copyright (2017) Elsevier. (d) CO₂ absorber with microchannel mesh structure. Adapted with permission from Ref. [198], copyright (2010) American Chemical Society. (e) Mesh contactor with SEM picture of the circle silicon nitride mesh. Adapted with permission from Ref. [199], copyright (2012) Elsevier. (f) Honeycomb fractal-type CO₂ absorber. Adapted with permission from Ref. [200], copyright (2018) Elsevier. (g) TPMS structure based CO₂ absorber. Reproduced with permission from Ref. [201], copyright (2022) Elsevier. (h) gyroid structure based CO₂ membrane absorber. Reproduced with permission from Ref. [203], copyright (2021) Elsevier.

Table 5 Summary of intensification measures to improve the CO₂ absorption performance in microchannel-based reactors

Working fluids	Microchannel geometry and dimension	Two-phase flow pattern	Intensification measures	Performance enhancement wrt. reference channel	Energy consumption/pressure drop	Ref.
DEA+CO ₂ NaOH+CO ₂	Flat microchannel with a 1 μm thickness silicon nitride mesh	Co-current and counter-current flow	Silicon nitride mesh contactor	30% CO ₂ absorbed for contact time less than 0.5 s		[199]
DI water+CO ₂	Rectangular serpentine microchannel (1 mm×1 mm)	Slug-bubbly	Serpentine geometry + high-power ultrasonic	$K_L a$ increased by 5.7 times	Power input: 100W	[41]
DEA+CO ₂	16 parallel rectangular microchannel (600 μm×300 μm)	Taylor-bubbly	Multiple channel collection + serpentine geometry + high system pressure	k_L^0 increased by 1-2 orders of magnitude	Maximum Δp: 0.45 MPa ($Re_L=1500$, $Q_{GS}=0.1$ L/min)	[115]
MDEA+CO ₂	Circular serpentine microchannel ($d_h=800$ μm)	Bubbly	Serpentine geometry + ultrasonic	$k_L a$ 10 times higher than conventional reactor	Power input: 100W	[180]
MEA/[Bmim][BF ₄] aqueous solution+CO ₂	Rectangular straight microchannel (800 μm×400 μm)	Taylor bubbly	Micro baffle obstacles	$k_L a$ increased by 50%	Maximum Δp: 2.5 kPa	[57]
MEA+CO ₂ +nickel nanoparticles	Rectangular serpentine microchannel (100 μm×50 μm)	Bubbly	Serpentine geometry + NiNPs catalyst	η_{CO_2} increased by 54%		[167]
Sodium glycinate aqueous solution+CO ₂	4 parallel rectangular microchannels (400 μm×400 μm)	Taylor bubbly	multiple channel collection	η_{CO_2} reached 80%-100%, average $k_L a_v$ reached 3-4 m ⁻¹	Δp ranging from 0.63 to 6.7 kPa	[195]
DI water+CO ₂	Rectangular straight microchannel (800 μm×800 μm, 600 μm×600 μm and 400 μm×400 μm)	Slug	Micro rectangular baffle obstacles	$k_L a$ increased by up to 180%	Maximum Δp: 6 kPa ($U_G=0.25$ m/s, $U_L=0.069$ m/s)	[175]
[Bmim][BF ₄] aqueous solution+CO ₂	Rectangular straight microchannel (400 μm×400 μm)	Bubbly	Continuous sudden expansion units inside the microchannel	$k_L a$ increased by 240%	Total Δp smaller than 4.5 kPa ($Q_L=30$ ml/h, $Q_G=180$ ml/h)	[59]
Potassium carbonate solution+CO ₂	Rectangular serpentine microchannel (1000 μm×1000 μm)	Slug bubbly	Special serpentine geometry+SiO ₂ particles	$k_L a$ increased by 30%	Δp ranging from 0.26 to 3.49 kPa	[108]
[Bmim][BF ₄] aqueous solution+CO ₂	Rectangular straight microchannel (800 μm×400 μm)	Taylor	Heart-shaped grooves inside the microchannel	$k_L a$ increased by 220%	Δp ranging from 1.5 to 3.7 kPa	[35]
MEA+CO ₂	Serpentine rectangular microchannel (600μm×600μm)	Taylor	Special serpentine geometry	$k_L a$ increased by 120%		[40]

6. Conclusion and prospects

This work provides an extensive review on the chemical absorption of CO₂ using microfluidic devices. The main findings may be summarized as follows.

- Microfluidic-based CO₂ chemical absorption technology has shown to exhibit various advantages compared to large-size conventional equipment, e.g., at least 1 or 2 orders of magnitude higher liquid-side volumetric mass transfer coefficient and interfacial area.
- The absorption of CO₂ in slug/bubbly two-phase flow pattern in microchannel using high-performance absorbents is an effective way to perform the CO₂ capture. The mass transfer between the gas bubble and the liquid phase determines the absorption performance in microchannel.
- Two-film model and unit-cell model are generally used for the mass transfer modeling. Besides, some dimensionless number-based empirical correlations are used for a fast estimation of mass transfer performance. Better prediction may be achieved by introducing chemical reaction and structure factors into the correlations.
- Gas and liquid flowrates and the solvent concentration have important impact on the absorption while the influence of working temperature is relatively minor. The elevated system pressure may have a negative impact on the $K_G a$, but can improve the overall η_{CO_2} and decrease the pressure drop (energy dissipation).
- Measuring local & interfacial parameters by using the non-intrusive optical-based techniques (e.g., LFD, LIF, PIV, etc.) is very meaningful for understanding the mechanisms of transport phenomena and for the development of new models. The local and transient characteristics obtained can also provide useful insights for the structural optimization of the microchannel.
- Different measures were proposed to enhance the CO₂ mass transfer in microchannel-based reactor, at the cost of additional energy consumption. Compared with external energy input, the structural modification method seems to be more economic. Furthermore, the combination of two or several intensification measures could be a promising strategy.
- The CO₂ processing capacity can be multiplied by adopting proper integration of microchannels, such as parallelization, meshed network, lattice structure, etc. Nevertheless, the uneven distribution of gas-liquid flow remains as an obstacle to overcome for such scaling-up strategy.'

These findings well illustrate both the potential and the current limitations of the microfluidic-based CO₂ chemical absorption technology. Great efforts are still needed to overcome the scientific and technological barriers for the widespread application of microchannel-based CO₂ capture technology in different industry sectors. Some of the remaining challenging issues include but not limited to:

- To develop new and efficient absorbents with low regeneration energy consumption, low corrosiveness and low solvent loss during cyclic operations.

- To improve and develop CO₂ mass transfer models in microchannel based on the accurate and transient information of two-phase flow dynamics and CO₂ concentration field in microchannel, obtained by advanced numerical and measuring techniques.
- To better understand the reaction mechanisms/kinetics and the corresponding heat transfer characteristics, which is largely insufficient at this stage.
- To search for the effective structuration of microchannel geometry based on the advanced modeling, optimization algorithms, and experimental verification, taking the fluid flow and coupled heat and mass transfer into account.
- To design and develop macro-sized, locally microfluidic-based devices possessing both the high CO₂ absorption performance and high throughput of CO₂ treatment, and their realization by advanced additive manufacturing method.
- Scaling-up of microfluidic-based CO₂ absorbers and their field testing with post-combustion gases[204,205] under realistic operation conditions (e.g., high temperature and pressure, gas mixture, etc.). The cost estimation and economic analysis will help showcase the commercialization potential and the competitiveness of such technology for the carbon capture duties in different industrial sectors.

Acknowledgement

This work is supported by the French Ministry of Europe and Foreign Affairs (Ministère de l'Europe et des Affaires Étrangères) through the PHC Xu Guangqi program (No.45614RM, 2020), and by the China Scholarship Council with the scholarship for Mr. Hao CHENG (No. 20200673006). For their permission to reproduce the figures, we thank the ACS, Wiley, American Chemical Society and Elsevier.

References

- [1] Yoro KO, Daramola MO. CO₂ emission sources, greenhouse gases, and the global warming effect. *Adv. carbon capture*, Elsevier; 2020, p. 3–28.
- [2] Ritchie H, Roser M, Rosado P. CO₂ and greenhouse gas emissions. *Our World Data* 2020.
- [3] Dr. Pieter Tans, NOAA/GML (gml.noaa.gov/ccgg/trends/) and Dr. Ralph Keeling, Scripps Institution of Oceanography (scrippsco2.ucsd.edu/).
- [4] Quesada BR. United Nations' Intergovernmental Panel on Climate Change's (IPCC) Special Report on Climate Change and Land (SRCCL)-Chapter 2: Land-Climate Interactions. *Land-Climate Interact* 2019.
- [5] Pasha M, Liu S, Zhang J, Qiu M, Su Y. Recent Advancements on Hydrodynamics and Mass Transfer Characteristics for CO₂ Absorption in Microreactors. *Ind Eng Chem Res* 2022.
- [6] Ke-Jun J, Sheng-Bo F. Going to the mitigation targets in Paris Agreement: the world is on the road. *Adv Clim Chang Res* 2021;17:1.
- [7] Höhne N, Gidden MJ, den Elzen M, Hans F, Fyson C, Geiges A, et al. Wave of net zero emission targets opens window to meeting the Paris Agreement. *Nat Clim Chang* 2021;11:820–2.
- [8] Rahman FA, Aziz MMA, Saidur R, Bakar WAWA, Hainin MR, Putrajaya R, et al. Pollution to solution: Capture and sequestration of carbon dioxide (CO₂) and its utilization as a renewable energy source for a sustainable future. *Renew Sustain Energy Rev* 2017;71:112–26.
- [9] Kiatkittipong K, Mohamad Shukri MAA, Kiatkittipong W, Lim JW, Show PL, Lam MK, et al. Green pathway in utilizing CO₂ via cycloaddition reaction with epoxide—a mini review. *Processes* 2020;8:548.
- [10] Chao C, Deng Y, Dewil R, Baeyens J, Fan X. Post-combustion carbon capture. *Renew Sustain Energy Rev* 2021;138:110490.
- [11] Ghaib K, Ben-Fares F-Z. Power-to-Methane: A state-of-the-art review. *Renew Sustain Energy Rev* 2018;81:433–46.
- [12] Davison J. Performance and costs of power plants with capture and storage of CO₂. *Energy* 2007;32:1163–76.
- [13] Li W, Zhao X, Liu B, Tang Z. Mass transfer coefficients for CO₂ absorption into aqueous ammonia using structured packing. *Ind Eng Chem Res* 2014;53:6185–96. <https://doi.org/10.1021/ie403097h>.
- [14] Hepburn C, Adlen E, Beddington J, Carter EA, Fuss S, Mac Dowell N, et al. The technological and economic prospects for CO₂ utilization and removal. *Nature* 2019;575:87–97.
- [15] Janati S, Aghel B, Shadloo MS. The effect of alkanolamine mixtures on CO₂ absorption efficiency in T-Shaped microchannel. *Environ Technol Innov* 2021:102006.
- [16] Jajja SA, Sequeira JM, Fronk BM. Geometry and orientation effects in non-uniformly heated microchannel heat exchangers using supercritical carbon dioxide. *Exp Therm Fluid Sci* 2020;112:109979.
- [17] Cui P, Wang S. Application of microfluidic chip technology in pharmaceutical analysis: A review. *J Pharm Anal* 2019;9:238–47.
- [18] Chen J, Chen D, Xie Y, Yuan T, Chen X. Progress of microfluidics for biology and medicine. *Nano-Micro Lett* 2013;5:66–80.
- [19] Afzal MJ, Ashraf MW, Tayyaba S, Hossain MK, Afzulpurkar N. Sinusoidal microchannel with descending curves for varicose veins implantation. *Micromachines* 2018;9:59.
- [20] Koronaki IP, Prentza L, Papaefthimiou V. Modeling of CO₂ capture via chemical absorption processes— An extensive literature review. *Renew Sustain Energy Rev* 2015;50:547–66.
- [21] Dinca C, Slavu N, Badea A. Benchmarking of the pre/post-combustion chemical absorption for the CO₂ capture. *J Energy Inst* 2018;91:445–56.
- [22] Sattari A, Ramazani A, Aghahosseini H, Aroua MK. The application of polymer containing materials in CO₂ capturing via absorption and adsorption methods. *J CO₂ Util* 2021;48:101526.
- [23] Zhu X, Xie W, Wu J, Miao Y, Xiang C, Chen C, et al. Recent advances in direct air capture by adsorption. *Chem Soc Rev* 2022.
- [24] Liu R, Shi X, Wang C, Gao Y, Xu S, Hao G, et al. Advances in post-combustion CO₂ capture by physical adsorption: from materials innovation to separation practice. *ChemSusChem* 2021;14:1428–71.
- [25] Xie K, Fu Q, Qiao GG, Webley PA. Recent progress on fabrication methods of polymeric thin film gas separation membranes for CO₂ capture. *J Memb Sci* 2019;572:38–60.
- [26] Zhu B, Jiang X, He S, Yang X, Long J, Zhang Y, et al. Rational design of poly (ethylene oxide) based membranes for sustainable CO₂ capture. *J Mater Chem A* 2020;8:24233–52.
- [27] Yousef AM, El-Maghlany WM, Eldrainy YA, Attia A. New approach for biogas purification using cryogenic separation and distillation process for CO₂ capture. *Energy* 2018;156:328–51.
- [28] Song C, Liu Q, Deng S, Li H, Kitamura Y. Cryogenic-based CO₂ capture technologies: State-of-the-art developments and current challenges. *Renew Sustain Energy Rev* 2019;101:265–78.
- [29] Daneshvar E, Wicker RJ, Show P-L, Bhatnagar A. Biologically-mediated carbon capture and utilization by microalgae towards sustainable CO₂ biofixation and biomass valorization—A review. *Chem Eng J* 2022;427:130884.
- [30] Cheng YW, Lim JSM, Chong CC, Lam MK, Lim JW, Tan IS, et al. Unravelling CO₂ capture performance of microalgae cultivation and other technologies via comparative carbon balance analysis. *J Environ Chem Eng* 2021;9:106519.
- [31] Wong YY, Rawindran H, Lim JW, Tiong ZW, Liew CS, Lam MK, et al. Attached microalgae converting spent coffee ground into lipid for biodiesel production and sequestering atmospheric CO₂ simultaneously. *Algal Res* 2022;66:102780.

- [32] Kumar G, Mondal TK, Kundu M. Solubility of CO₂ in aqueous blends of (Diethanolamine+ 2-amino-2-methyl-1-propanol) and (diethanolamine+ N-Methyl-diethanolamine). *J Chem Eng Data* 2012;57:670–80.
- [33] Horng S-Y, Li M-H. Kinetics of absorption of carbon dioxide into aqueous solutions of monoethanolamine+ triethanolamine. *Ind Eng Chem Res* 2002;41:257–66.
- [34] Choi W-J, Seo J-B, Jang S-Y, Jung J-H, Oh K-J. Removal characteristics of CO₂ using aqueous MEA/AMP solutions in the absorption and regeneration process. *J Environ Sci* 2009;21:907–13.
- [35] Chen Y, Zhu C, Fu T, Ma Y. Mass transfer enhancement of CO₂ absorption into [Bmim][BF₄] aqueous solution in microchannels by heart-shaped grooves. *Chem Eng Process - Process Intensif* 2021;167:108536. <https://doi.org/10.1016/j.cep.2021.108536>.
- [36] Maceiras R, Álvarez E, Cancela MÁ. Effect of temperature on carbon dioxide absorption in monoethanolamine solutions. *Chem Eng J* 2008;138:295–300. <https://doi.org/10.1016/j.cej.2007.05.049>.
- [37] Yue J, Chen G, Yuan Q, Luo L, Gonthier Y. Hydrodynamics and mass transfer characteristics in gas-liquid flow through a rectangular microchannel. *Chem Eng Sci* 2007;62:2096–108. <https://doi.org/10.1016/j.ces.2006.12.057>.
- [38] Yin Y, Zhu C, Guo R, Fu T, Ma Y. Gas-liquid two-phase flow in a square microchannel with chemical mass transfer: Flow pattern, void fraction and frictional pressure drop. *Int J Heat Mass Transf* 2018;127:484–96. <https://doi.org/10.1016/j.ijheatmasstransfer.2018.07.113>.
- [39] Darde V, Van Well WJM, Fosboel PL, Stenby EH, Thomsen K. Experimental measurement and modeling of the rate of absorption of carbon dioxide by aqueous ammonia. *Int J Greenh Gas Control* 2011;5:1149–62.
- [40] Zhou Y, Yao C, Zhang P, Zhang X, Lü H, Zhao Y. Dynamic coupling of mass transfer and chemical reaction for Taylor flow along a serpentine microchannel. *Ind Eng Chem Res* 2020;59:9279–92.
- [41] Dong Z, Yao C, Zhang X, Xu J, Chen G, Zhao Y, et al. A high-power ultrasonic microreactor and its application in gas-liquid mass transfer intensification. *Lab Chip* 2015;15:1145–52.
- [42] Afzal MJ, Tayyaba S, Ashraf MW, Khan MI, Javaid F, Basher MK, et al. A Review on Microchannel Fabrication Methods and Applications in Large-Scale and Prospective Industries 2022.
- [43] Yao C, Zhao Y, Ma H, Liu Y, Zhao Q, Chen G. Two-phase flow and mass transfer in microchannels: A review from local mechanism to global models. *Chem Eng Sci* 2021;229:116017.
- [44] Mumford KA, Wu Y, Smith KH, Stevens GW. Review of solvent based carbon-dioxide capture technologies. *Front Chem Sci Eng* 2015;9:125–41.
- [45] Zhang L, Zhang B, Yang Z, Guo M. The Role of Water on the Performance of Calcium Oxide-Based Sorbents for Carbon Dioxide Capture: A Review. *Energy Technol* 2015;3:10–9.
- [46] Hu G, Nicholas NJ, Smith KH, Mumford KA, Kentish SE, Stevens GW. Carbon dioxide absorption into promoted potassium carbonate solutions: A review. *Int J Greenh Gas Control* 2016;53:28–40.
- [47] Aghaie M, Rezaei N, Zendejboudi S. A systematic review on CO₂ capture with ionic liquids: Current status and future prospects. *Renew Sustain Energy Rev* 2018;96:502–25.
- [48] Gautam A, Mondal MK. Review of recent trends and various techniques for CO₂ capture: Special emphasis on biphasic amine solvents. *Fuel* 2023;334:126616.
- [49] Meng F, Meng Y, Ju T, Han S, Lin L, Jiang J. Research progress of aqueous amine solution for CO₂ capture: A review. *Renew Sustain Energy Rev* 2022;168:112902.
- [50] Ochedi FO, Yu J, Yu H, Liu Y, Hussain A. Carbon dioxide capture using liquid absorption methods: a review. *Environ Chem Lett* 2021;19:77–109.
- [51] Sattari-Najafabadi M, Esfahany MN, Wu Z, Sunden B. Mass transfer between phases in microchannels: A review. *Chem Eng Process Intensif* 2018;127:213–37.
- [52] Abdeen FRH, Mel M, Jami MS, Ihsan SI, Ismail AF. A review of chemical absorption of carbon dioxide for biogas upgrading. *Chinese J Chem Eng* 2016;24:693–702.
- [53] Borhan A, Yusup S, Lim JW, Show PL. Characterization and modelling studies of activated carbon produced from rubber-seed shell using KOH for CO₂ adsorption. *Processes* 2019;7:855.
- [54] Aghel B, Janati S, Wongwises S, Shadloo MS. Review on CO₂ capture by blended amine solutions. *Int J Greenh Gas Control* 2022;119:103715.
- [55] Yunus NM, Halim NH, Wilfred CD, Murugesan T, Lim JW, Show PL. Thermophysical properties and CO₂ absorption of ammonium-based protic ionic liquids containing acetate and butyrate anions. *Processes* 2019;7:820.
- [56] Jiang W, Li X, Gao G, Wu F, Luo C, Zhang L. Advances in applications of ionic liquids for phase change CO₂ capture. *Chem Eng J* 2022:136767.
- [57] Yin Y, Zhu C, Fu T, Ma Y, Wang K, Luo G. Enhancement effect and mechanism of gas-liquid mass transfer by baffles embedded in the microchannel. *Chem Eng Sci* 2019;201:264–73.
- [58] Yin Y, Chen W, Wu C, Zhang X, Fu T, Zhu C, et al. Bubble dynamics and mass transfer enhancement in split-and-recombine (SAR) microreactor with rapid chemical reaction. *Sep Purif Technol* 2022:120573.
- [59] Zhang S, Zhu C, Feng H, Fu T, Ma Y. Intensification of gas-liquid two-phase flow and mass transfer in microchannels by sudden expansions. *Chem Eng Sci* 2021;229:116040.
- [60] Zhang T, Cao B, Fan Y, Gonthier Y, Luo L, Wang S. Gas-liquid flow in circular microchannel. Part I: Influence of liquid physical properties and channel diameter on flow patterns. *Chem Eng Sci* 2011;66:5791–803.
- [61] Ma D, Zhu C, Fu T, Yuan X, Ma Y. An effective hybrid solvent of MEA/DEEA for CO₂ absorption and its mass transfer performance in microreactor. *Sep Purif Technol* 2020;242:116795.
- [62] Yin Y, Zhu C, Guo R, Fu T, Ma Y. Gas-liquid two-phase flow in a square microchannel with chemical mass transfer:

- Flow pattern, void fraction and frictional pressure drop. *Int J Heat Mass Transf* 2018;127:484–96.
- [63] Afzal MJ, Tayyaba S, Ashraf MW, Hossain MK, Uddin MJ, Afzulpurkar N. Simulation, fabrication and analysis of silver based ascending sinusoidal microchannel (ASMC) for implant of varicose veins. *Micromachines* 2017;8:278.
- [64] Nayak R, Lobo OJ, Chatterjee D, Das SK. Effect of geometrical parameters on slug behaviour and two phase pressure drop in microchannel T-junctions. *Chem Eng Process Intensif* 2018;130:76–87.
- [65] Choi CW, Yu DI, Kim MH. Adiabatic two-phase flow in rectangular microchannels with different aspect ratios: Part II–bubble behaviors and pressure drop in single bubble. *Int J Heat Mass Transf* 2010;53:5242–9.
- [66] Cantu-Perez A, Ziegenbalg D, Löb P, Gavriilidis A, Hessel V, Schönfeld F. Microstructure-based intensification of a falling film microreactor through optimal film setting with realistic profiles and in-channel induced mixing. *Chem Eng J* 2012;179:318–29.
- [67] Kawahara A, Chung P-Y, Kawaji M. Investigation of two-phase flow pattern, void fraction and pressure drop in a microchannel. *Int J Multiph Flow* 2002;28:1411–35.
- [68] El Hajal J, Thome JR, Cavallini A. Condensation in horizontal tubes, part 1: two-phase flow pattern map. *Int J Heat Mass Transf* 2003;46:3349–63.
- [69] Kong R, Kim S, Bajorek S, Tien K, Hoxie C. Effects of pipe size on horizontal two-phase flow: Flow regimes, pressure drop, two-phase flow parameters, and drift-flux analysis. *Exp Therm Fluid Sci* 2018;96:75–89.
- [70] Yue J, Luo L, Gonthier Y, Chen G, Yuan Q. An experimental investigation of gas–liquid two-phase flow in single microchannel contactors. *Chem Eng Sci* 2008;63:4189–202.
- [71] Ganapathy H, Shoostari A, Dessiatoun S, Ohadi MM, Alshehhi M. Hydrodynamics and mass transfer performance of a microreactor for enhanced gas separation processes. *Chem Eng J* 2015;266:258–70.
- [72] Khan W, Chandra AK, Kishor K, Sachan S, Alam MS. Slug formation mechanism for air–water system in T-junction microchannel: a numerical investigation. *Chem Pap* 2018;72:2921–32. <https://doi.org/10.1007/s11696-018-0522-7>.
- [73] Nekouei M, Vanapalli SA. Volume-of-fluid simulations in microfluidic T-junction devices: Influence of viscosity ratio on droplet size Mehdi Nekouei and Siva A. Vanapalli Department of Chemical Engineering, Texas Tech University, Lubbock, TX, 79409, USA 2017;032007:1–22.
- [74] Tan J, Lu YC, Xu JH, Luo GS. Mass transfer characteristic in the formation stage of gas–liquid segmented flow in microchannel. *Chem Eng J* 2012;185:314–20.
- [75] Ma D, Zhu C, Fu T, Ma Y, Yuan X. Synergistic effect of functionalized ionic liquid and alkanolamines mixed solution on enhancing the mass transfer of CO₂ absorption in microchannel. *Chem Eng J* 2021;417:129302.
- [76] Aghel B, Heidaryan E, Sahraie S, Nazari M. Optimization of monoethanolamine for CO₂ absorption in a microchannel reactor. *J CO₂ Util* 2018;28:264–73.
- [77] Lim AE, Lim CY, Lam YC, Lim YH. Effect of microchannel junction angle on two-phase liquid-gas Taylor flow. *Chem Eng Sci* 2019;202:417–28.
- [78] Deleau T, Fechter MHH, Letourneau J-J, Camy S, Aubin J, Braeuer AS, et al. Determination of mass transfer coefficients in high-pressure two-phase flows in capillaries using Raman spectroscopy. *Chem Eng Sci* 2020;228:115960.
- [79] Van Elk EP, Knaap MC, Versteeg GF. Application of the penetration theory for gas–liquid mass transfer without liquid bulk: Differences with systems with a bulk. *Chem Eng Res Des* 2007;85:516–24.
- [80] Higbie R. The rate of absorption of a pure gas into a still liquid during short periods of exposure. *Trans AIChE* 1935;31:365–89.
- [81] Cussler EL, Cussler EL. *Diffusion: mass transfer in fluid systems*. Cambridge university press; 2009.
- [82] Kashid MN, Renken A, Kiwi-Minsker L. Gas-liquid and liquid-liquid mass transfer in microstructured reactors. *Chem Eng Sci* 2011;66:3876–97. <https://doi.org/10.1016/j.ces.2011.05.015>.
- [83] Whitwell JC. *Gas Absorption in Flow Systems: Discussion of the Two Film Theory and the Experimental Effects of Varying Gas Velocity (through a Wide Range), Water Velocity, Concentration of Solute Gas and Inert Gas* 1932.
- [84] Chen X. *Carbon dioxide thermodynamics, kinetics, and mass transfer in aqueous piperazine derivatives and other amines* 2011.
- [85] Zeng Q, Guo Y, Niu Z, Lin W. Mass transfer coefficients for CO₂ absorption into aqueous ammonia solution using a packed column. *Ind Eng Chem Res* 2011;50:10168–75. <https://doi.org/10.1021/ie101821b>.
- [86] Jaffré J, Sboui A. Henry’ law and gas phase disappearance. *Transp Porous Media* 2010;82:521–6. <https://doi.org/10.1007/s11242-009-9407-0>.
- [87] Jepsen JC. Mass transfer in two-phase flow in horizontal pipelines. *AIChE J* 1970;16:705–11.
- [88] Yue J, Chen G, Yuan Q, Luo L, Le Gall H. 微通道内气-液传质研究 (Mass transfer in gas-liquid flow in microchannels). *CIESC J* 2006;57:1296–303.
- [89] Guo R, Zhu C, Yin Y, Fu T, Ma Y. Mass transfer characteristics of CO₂ absorption into 2-amino-2-methyl-1-propanol non-aqueous solution in a microchannel. *J Ind Eng Chem* 2019;75:194–201.
- [90] Yang L, Tan J, Wang K, Luo G. Mass transfer characteristics of bubbly flow in microchannels. *Chem Eng Sci* 2014;109:306–14.
- [91] Ji XY, Ma YG, Fu TT, Zhu CH, Wang DJ. Experimental investigation of the liquid volumetric mass transfer coefficient for upward gas-liquid two-phase flow in rectangular microchannels. *Brazilian J Chem Eng* 2010;27:573–82.
- [92] Niu H, Pan L, Su H, Wang S. Flow pattern, pressure drop, and mass transfer in a gas– liquid concurrent two-phase flow microchannel reactor. *Ind Eng Chem Res* 2009;48:1621–8.

- [93] Li C, Zhu C, Ma Y, Liu D, Gao X. Experimental study on volumetric mass transfer coefficient of CO₂ absorption into MEA aqueous solution in a rectangular microchannel reactor. *Int J Heat Mass Transf* 2014;78:1055–9.
- [94] Yin Y, Fu T, Zhu C, Guo R, Ma Y, Li H. Dynamics and mass transfer characteristics of CO₂ absorption into MEA/[Bmim][BF₄] aqueous solutions in a microchannel. *Sep Purif Technol* 2019;210:541–52.
- [95] Zhang Y, Zhu C, Chu C, Fu T, Ma Y. Mass transfer and capture of carbon dioxide using amino acids sodium aqueous solution in microchannel. *Chem Eng Process Intensif* 2022;173:108831.
- [96] Chu C, Zhang F, Zhu C, Fu T, Ma Y. Mass transfer characteristics of CO₂ absorption into 1-butyl-3-methylimidazolium tetrafluoroborate aqueous solution in microchannel. *Int J Heat Mass Transf* 2019;128:1064–71.
- [97] Niu H, Pan L, Su H, Wang S. Effects of design and operating parameters on CO₂ absorption in microchannel contactors. *Ind Eng Chem Res* 2009;48:8629–34.
- [98] Ganapathy H, Shooshtari A, Dessiatoun S, Alshehhi M, Ohadi M. Fluid flow and mass transfer characteristics of enhanced CO₂ capture in a minichannel reactor. *Appl Energy* 2014;119:43–56.
- [99] Pan M-Y, Qian Z, Shao L, Arowo M, Chen J-F, Wang J-X. Absorption of carbon dioxide into N-methyldiethanolamine in a high-throughput microchannel reactor. *Sep Purif Technol* 2014;125:52–8.
- [100] Kittiampon N, Kaewchada A, Jaree A. Carbon dioxide absorption using ammonia solution in a microchannel. *Int J Greenh Gas Control* 2017;63:431–41.
- [101] Liu H, Yao C, Zhao Y, Chen G. Heat Transfer Characteristics of CO₂ Desorption from N-Methyldiethanolamine Solution in a Microchannel Reactor. *Chem Eng Technol* 2018;41:1398–405.
- [102] Lin G, Jiang S, Zhu C, Fu T, Ma Y. Mass-transfer characteristics of CO₂ absorption into aqueous solutions of N-methyldiethanolamine+ diethanolamine in a T-junction microchannel. *ACS Sustain Chem Eng* 2019;7:4368–75.
- [103] Aghel B, Heidaryan E, Sahraie S, Mir S. Application of the microchannel reactor to carbon dioxide absorption. *J Clean Prod* 2019;231:723–32.
- [104] Aghel B, Sahraie S, Heidaryan E. Comparison of aqueous and non-aqueous alkanolamines solutions for carbon dioxide desorption in a microreactor. *Energy* 2020;201:117618.
- [105] Aghel B, Sahraie S, Heidaryan E. Carbon dioxide desorption from aqueous solutions of monoethanolamine and diethanolamine in a microchannel reactor. *Sep Purif Technol* 2020;237:116390.
- [106] Wang J, Li H, Li X, Cong H, Gao X. An intensification of mass transfer process for gas-liquid counter-current flow in a novel microchannel with limited path for CO₂ capture. *Process Saf Environ Prot* 2021;149:905–14.
- [107] Huang M, Zhu C, Fu T, Ma Y. Enhancement of gas-liquid mass transfer by nanofluids in a microchannel under Taylor flow regime. *Int J Heat Mass Transf* 2021;176:121435.
- [108] Pang Z, Jiang S, Zhu C, Ma Y, Fu T. Mass transfer of chemical absorption of CO₂ in a serpentine minichannel. *Chem Eng J* 2021;414:128791.
- [109] Yin Y, Zhang X, Zhu C, Fu T, Ma Y. Formation characteristics of Taylor bubbles in a T-junction microchannel with chemical absorption. *Chinese J Chem Eng* 2021.
- [110] Pasha M, Zhang H, Shang M, Li G, Su Y. CO₂ absorption with diamine functionalized deep eutectic solvents in microstructured reactors. *Process Saf Environ Prot* 2022;159:106–19.
- [111] Dandapat BS, Santra B, Andersson HI. Thermocapillarity in a liquid film on an unsteady stretching surface. *Int J Heat Mass Transf* 2003;46:3009–15.
- [112] Ye C, Dang M, Yao C, Chen G, Yuan Q. Process analysis on CO₂ absorption by monoethanolamine solutions in microchannel reactors. *Chem Eng J* 2013;225:120–7.
- [113] Zhang Z, Cai J, Chen F, Li H, Zhang W, Qi W. Progress in enhancement of CO₂ absorption by nanofluids: A mini review of mechanisms and current status. *Renew Energy* 2018;118:527–35.
- [114] Zaloha P, Kristal J, Jiricny V, Völkel N, Xuereb C, Aubin J. Characteristics of liquid slugs in gas–liquid Taylor flow in microchannels. *Chem Eng Sci* 2012;68:640–9.
- [115] Yao C, Zhu K, Liu Y, Liu H, Jiao F, Chen G. Intensified CO₂ absorption in a microchannel reactor under elevated pressures. *Chem Eng J* 2017;319:179–90.
- [116] Aroonwilas A, Tontiwachwuthikul P. High-efficiency structured packing for CO₂ separation using 2-amino-2-methyl-1-propanol (AMP). *Sep Purif Technol* 1997;12:67–79.
- [117] Zeng Q, Guo Y, Niu Z, Lin W. Mass transfer coefficients for CO₂ absorption into aqueous ammonia solution using a packed column. *Ind Eng Chem Res* 2011;50:10168–75.
- [118] Freeman SA, Dugas R, Van Wagener DH, Nguyen T, Rochelle GT. Carbon dioxide capture with concentrated, aqueous piperazine. *Int J Greenh Gas Control* 2010;4:119–24.
- [119] Li L, Voice AK, Li H, Namjoshi O, Nguyen T, Du Y, et al. Amine blends using concentrated piperazine. *Energy Procedia* 2013;37:353–69.
- [120] Li H, Li L, Nguyen T, Rochelle GT, Chen J. Characterization of piperazine/2-aminomethylpropanol for carbon dioxide capture. *Energy Procedia* 2013;37:340–52.
- [121] Conway W, Bruggink S, Beyad Y, Luo W, Melián-Cabrera I, Puxty G, et al. CO₂ absorption into aqueous amine blended solutions containing monoethanolamine (MEA), N, N-dimethylethanolamine (DMEA), N, N-diethylethanolamine (DEEA) and 2-amino-2-methyl-1-propanol (AMP) for post-combustion capture processes. *Chem Eng Sci* 2015;126:446–54.
- [122] Chen H, Dou B, Song Y, Xu Y, Wang X, Zhang Y, et al. Studies on absorption and regeneration for CO₂ capture by aqueous ammonia. *Int J Greenh Gas Control* 2012;6:171–8.
- [123] Akkarawatkhosith N, Nopcharoenkul W, Kaewchada A, Jaree A. Mass Transfer Correlation and Optimization of

- Carbon Dioxide Capture in a Microchannel Contactor: A Case of CO₂-Rich Gas. *Energies* 2020;13:5465.
- [124] Akkarawatkhooisith N, Kaewchada A, Jaree A. High-throughput CO₂ capture for biogas purification using monoethanolamine in a microtube contactor. *J Taiwan Inst Chem Eng* 2019;98:113–23.
- [125] Aghel B, Gouran A, Behaein S. Intensified biogas upgrading via various wastewater using microchannel. *Chem Eng Process Intensif* 2022:108927.
- [126] Rivera-Tinoco R, Bouallou C. Comparison of absorption rates and absorption capacity of ammonia solvents with MEA and MDEA aqueous blends for CO₂ capture. *J Clean Prod* 2010;18:875–80.
- [127] Ge X, Shaw SL, Zhang Q. Toward understanding amines and their degradation products from postcombustion CO₂ capture processes with aerosol mass spectrometry. *Environ Sci Technol* 2014;48:5066–75.
- [128] Leung SSY, Liu Y, Fletcher DF, Haynes BS. Heat transfer in well-characterised Taylor flow. *Chem Eng Sci* 2010;65:6379–88.
- [129] Van Baten JM, Krishna R. CFD simulations of mass transfer from Taylor bubbles rising in circular capillaries. *Chem Eng Sci* 2004;59:2535–45.
- [130] Gupta R, Fletcher DF, Haynes BS. On the CFD modelling of Taylor flow in microchannels. *Chem Eng Sci* 2009;64:2941–50.
- [131] Mesquita LCS, Harrison SJ, Thomey D. Modeling of heat and mass transfer in parallel plate liquid-desiccant dehumidifiers. *Sol Energy* 2006;80:1475–82.
- [132] Jia HW, Zhang P. Investigation of the Taylor bubble under the effect of dissolution in microchannel. *Chem Eng J* 2016;285:252–63.
- [133] Han Y, Shikazono N. The effect of bubble acceleration on the liquid film thickness in micro tubes. *Int J Heat Fluid Flow* 2010;31:630–9.
- [134] Bartkus G V, Kuznetsov V V. Film thickness measurement for elongated bubble flow in microchannel using LIF. *MATEC Web Conf.*, vol. 84, EDP Sciences; 2016, p. 5.
- [135] Cheng H, Xian H, Zhou L, Du X. Experimental study on the oscillation characteristics of thin liquid film in a microchannel. *Exp Therm Fluid Sci* 2020;115:110089.
- [136] Fairbrother F, Stubbs AE. 119. Studies in electro-endosmosis. Part VI. The “bubble-tube” method of measurement. *J Chem Soc* 1935:527–9.
- [137] Taylor GI. Deposition of a viscous fluid on the wall of a tube. *J Fluid Mech* 1961;10:161–5.
- [138] Irandoust S, Andersson B. Simulation of flow and mass transfer in Taylor flow through a capillary. *Comput Chem Eng* 1989;13:519–26.
- [139] Aussillous P, Quéré D. Quick deposition of a fluid on the wall of a tube. *Phys Fluids* 2000;12:2367–71.
- [140] Heiszwolf JJ, Kreutzer MT, van den Eijnden MG, Kapteijn F, Moulijn JA. Gas–liquid mass transfer of aqueous Taylor flow in monoliths. *Catal Today* 2001;69:51–5.
- [141] Han Y, Shikazono N, Kasagi N. Measurement of liquid film thickness in a micro parallel channel with interferometer and laser focus displacement meter. *Int J Multiph Flow* 2011;37:36–45.
<https://doi.org/10.1016/j.ijmultiphaseflow.2010.08.010>.
- [142] Klaseboer E, Gupta R, Manica R. An extended Bretherton model for long Taylor bubbles at moderate capillary numbers. *Phys Fluids* 2014;26:32107.
- [143] Youn YJ, Muramatsu K, Han Y, Shikazono N. The effect of initial flow velocity on the liquid film thickness in micro tube accelerated slug flow. *Int J Multiph Flow* 2015;73:108–17.
- [144] Youn YJ, Muramatsu K, Han Y, Shikazono N. The effect of bubble deceleration on the liquid film thickness in microtubes. *Int J Heat Fluid Flow* 2016;58:84–92.
- [145] Ni D, Hong FJ, Cheng P, Chen G. Numerical study of liquid-gas and liquid-liquid Taylor flows using a two-phase flow model based on Arbitrary-Lagrangian–Eulerian (ALE) formulation. *Int Commun Heat Mass Transf* 2017;88:37–47.
- [146] Patel RS, Weibel JA, Garimella S V. Characterization of liquid film thickness in slug-regime microchannel flows. *Int J Heat Mass Transf* 2017;115:1137–43.
- [147] Soh GY, Yeoh GH, Timchenko V. Numerical investigation of formation and dissolution of CO₂ bubbles within silicone oil in a cross-junction microchannel. *Microfluid Nanofluidics* 2017;21:1–17.
- [148] Yang L, Nieves-Remacha MJ, Jensen KF. Simulations and analysis of multiphase transport and reaction in segmented flow microreactors. *Chem Eng Sci* 2017;169:106–16.
- [149] Abiev RS, Butler C, Cid E, Lalanne B, Billet A-M. Mass transfer characteristics and concentration field evolution for gas-liquid Taylor flow in milli channels. *Chem Eng Sci* 2019;207:1331–40.
- [150] Li W-L, Wang J-H, Lu Y-C, Shao L, Chu G-W, Xiang Y. CFD analysis of CO₂ absorption in a microporous tube-in-tube microchannel reactor with a novel gas-liquid mass transfer model. *Int J Heat Mass Transf* 2020;150:119389.
- [151] Dong R, Chu D, Sun Q, Jin Z. Numerical simulation of the mass transfer process of CO₂ absorption by different solutions in a microchannel. *Can J Chem Eng* 2020;98:2648–64.
- [152] Kuhn S, Jensen KF. A pH-sensitive laser-induced fluorescence technique to monitor mass transfer in multiphase flows in microfluidic devices. *Ind Eng Chem Res* 2012;51:8999–9006.
- [153] Dietrich N, Loubiere K, Jimenez M, Hebrard G, Gourdon C. A new direct technique for visualizing and measuring gas–liquid mass transfer around bubbles moving in a straight millimetric square channel. *Chem Eng Sci* 2013;100:172–82.
- [154] Deleau T, Letourneau JJ, Camy S, Aubin J, Espitalier F. Determination of mass transfer coefficients in high-pressure CO₂-H₂O flows in microcapillaries using a colorimetric method. *Chem Eng Sci* 2022;248:117161.

- [155] Ichiyanagi M, Tsutsui I, Kakinuma Y, Sato Y, Hishida K. Three-dimensional measurement of gas dissolution process in gas-liquid microchannel flow. *Int J Heat Mass Transf* 2012;55:2872–8.
- [156] Butler C, Lalanne B, Sandmann K, Cid E, Billet A-M. Mass transfer in Taylor flow: Transfer rate modelling from measurements at the slug and film scale. *Int J Multiph Flow* 2018;105:185–201.
- [157] Chen Y, Zhu C, Fu T, Ma Y. Mass transfer enhancement of CO₂ absorption into [Bmim][BF₄] aqueous solution in microchannels by heart-shaped grooves. *Chem Eng Process Intensif* 2021;167:108536.
- [158] Charogiannis A, An JS, Markides CN. A simultaneous planar laser-induced fluorescence, particle image velocimetry and particle tracking velocimetry technique for the investigation of thin liquid-film flows. *Exp Therm Fluid Sci* 2015;68:516–36.
- [159] Willems P, Deen NG, Kemperman AJB, Lammertink RGH, Wessling M, van Sint Annaland M, et al. Use of Particle Imaging Velocimetry to measure liquid velocity profiles in liquid and liquid/gas flows through spacer filled channels. *J Memb Sci* 2010;362:143–53.
- [160] Kováts P, Thévenin D, Zähringer K. Characterizing fluid dynamics in a bubble column aimed for the determination of reactive mass transfer. *Heat Mass Transf* 2018;54:453–61.
- [161] Azadi R, Nobes DS. Local flow dynamics in the motion of slug bubbles in a flowing mini square channel. *Int J Heat Mass Transf* 2021;178:121588.
- [162] Nivedita N, Ligrani P, Papautsky I. Dean flow dynamics in low-aspect ratio spiral microchannels. *Sci Rep* 2017;7:1–10.
- [163] Duryodhan VS, Chatterjee R, Singh SG, Agrawal A. Mixing in planar spiral microchannel. *Exp Therm Fluid Sci* 2017;89:119–27.
- [164] Yang L, Dietrich N, Loubière K, Gourdon C, Hébrard G. Visualization and characterization of gas-liquid mass transfer around a Taylor bubble right after the formation stage in microreactors. *Chem Eng Sci* 2016;143:364–8.
- [165] Yang L, Loubière K, Dietrich N, Le Men C, Gourdon C, Hébrard G. Local investigations on the gas-liquid mass transfer around Taylor bubbles flowing in a meandering millimetric square channel. *Chem Eng Sci* 2017;165:192–203.
- [166] Yao C, Liu Y, Zhao S, Dong Z, Chen G. Bubble/droplet formation and mass transfer during gas-liquid-liquid segmented flow with soluble gas in a microchannel. *AIChE J* 2017;63:1727–39.
- [167] Seo S, Lages B, Kim M. Catalytic CO₂ absorption in an amine solvent using nickel nanoparticles for post-combustion carbon capture. *J CO₂ Util* 2020;36:244–52.
- [168] Tan J, Lu YC, Xu JH, Luo GS. Mass transfer performance of gas-liquid segmented flow in microchannels. *Chem Eng J* 2012;181:229–35.
- [169] MacInnes JM, Ayash AA, Dowson GRM. CO₂ absorption using diethanolamine-water solutions in a rotating spiral contactor. *Chem Eng J* 2017;307:1084–91.
- [170] Sobieszuk P, Aubin J, Pohorecki R. Hydrodynamics and mass transfer in gas-liquid flows in microreactors. *Chem Eng Technol* 2012;35:1346–58.
- [171] Stroock AD, Dertinger SKW, Ajdari A, Mezić I, Stone HA, Whitesides GM. Chaotic mixer for microchannels. *Science* (80-) 2002;295:647–51.
- [172] Afzal A, Badruddin IA, Khan TMY, Kamangar S, Abdelmohimen M, Soudagar MEM, et al. Numerical investigation on pressure-driven electro osmotic flow and mixing in a constricted micro channel by triangular obstacle. *Int J Numer Methods Heat Fluid Flow* 2020.
- [173] He L, Fan Y, Bellettre J, Yue J, Luo L. Catalytic methane combustion in plate-type microreactors with different channel configurations: An experimental study. *Chem Eng Sci* 2021;236:116517.
- [174] Seo H-S, Kim Y-J. A study on the mixing characteristics in a hybrid type microchannel with various obstacle configurations. *Mater Res Bull* 2012;47:2948–51.
- [175] Yin Y, Guo R, Zhu C, Fu T, Ma Y. Enhancement of gas-liquid mass transfer in microchannels by rectangular baffles. *Sep Purif Technol* 2020;236:116306.
- [176] Chai L, Wang L, Zhou M, Xia G. Two-phase flow pattern and pressure drop in silicon multi-microchannel with expansion-constriction cross-section. *Exp Therm Fluid Sci* 2015;60:241–51.
- [177] Lü Y, Zhu S, Wang K, Luo G. Simulation of the mixing process in a straight tube with sudden changed cross-section. *Chinese J Chem Eng* 2016;24:711–8.
- [178] Zhang J, Lei L, Li H, Xin G, Wang X. Experimental and numerical studies of liquid-liquid two-phase flows in microchannel with sudden expansion/contraction cavities. *Chem Eng J* 2022;433:133820.
- [179] Lee JW, Kim S, Pineda IT, Kang YT. Review of nanoabsorbents for capture enhancement of CO₂ and its industrial applications with design criteria. *Renew Sustain Energy Rev* 2021;138:110524.
- [180] Liu H, Zhao S, Zhou F, Yao C, Chen G. Ultrasonic enhancement of CO₂ desorption from MDEA solution in microchannels. *Ind Eng Chem Res* 2019;58:1711–9.
- [181] Matin MH, Khan WA. Entropy generation analysis of heat and mass transfer in mixed electrokinetically and pressure driven flow through a slit microchannel. *Energy* 2013;56:207–17.
- [182] Zhao S, Yao C, Dong Z, Chen G, Yuan Q. Role of ultrasonic oscillation in chemical processes in microreactors: A mesoscale issue. *Particuology* 2020;48:88–99.
- [183] Wang C, Rallabandi B, Hilgenfeldt S. Frequency dependence and frequency control of microbubble streaming flows. *Phys Fluids* 2013;25:22002.
- [184] Dong Z, Yao C, Zhang Y, Chen G, Yuan Q, Xu J. Hydrodynamics and mass transfer of oscillating gas-liquid flow in

- ultrasonic microreactors. *AIChE J* 2016;62:1294–307.
- [185] Akbari M, Rahimi M, Faryadi M. Gas–liquid flow mass transfer in a T-shape microreactor stimulated with 1.7 MHz ultrasound waves. *Chinese J Chem Eng* 2017;25:1143–52.
- [186] Zhang Q, Dong Z, Zhao S, Liu Z, Chen G. Ultrasound-assisted gas–liquid mass transfer process in microreactors: the influence of surfactant, channel size and ultrasound frequency. *Chem Eng J* 2021;405:126720.
- [187] Hoseini N, Esfahany MN, Etesami N, Afarani HT, Fadaie E. INVESTIGATION OF THE EFFECT OF ELECTRIC FIELD ON CO₂ ABSORPTION IN WATER/Fe₃O₄ NANOFUID. *Brazilian J Chem Eng* 2019;36:1333–42.
- [188] Iliuta I, Larachi F. CO₂ and H₂S absorption by MEA solution in packed-bed columns under inclined and heaving motion conditions-Hydrodynamics and reactions performance for marine applications. *Int J Greenh Gas Control* 2018;79:1–13.
- [189] Laugier F, Andriantsiferana C, Wilhelm A-M, Delmas H. Ultrasound in gas–liquid systems: Effects on solubility and mass transfer. *Ultrason Sonochem* 2008;15:965–72.
- [190] Mc Carogher K, Dong Z, Stephens DS, Leblebici ME, Mettin R, Kuhn S. Acoustic resonance and atomization for gas-liquid systems in microreactors. *Ultrason Sonochem* 2021;75:105611.
- [191] Khmelev VN, Golykh RN, Bobrova GA, Shalunov A V, Shakura VA, Pedder V V. Mass Transfer Rate Increasing by Ultrasonic Oscillations in " Gas-Liquid" Systems. 2019 20th Int. Conf. Young Spec. Micro/Nanotechnologies Electron Devices, IEEE; 2019, p. 231–4.
- [192] Zhou P, Tarlet D, Fan Y, Hu X, Luo L. Water-in-oil emulsification in a bifurcated tree-like network: Flow distribution properties and their impact on the emulsion polydispersity. *Chem Eng Res Des* 2018;134:420–33.
- [193] Tarlet D, Fan Y, Roux S, Luo L. Entropy generation analysis of a mini heat exchanger for heat transfer intensification. *Exp Therm Fluid Sci* 2014;53. <https://doi.org/10.1016/j.expthermflusci.2013.11.016>.
- [194] Yue J, Boichot R, Luo L, Gonthier Y, Chen G, Yuan Q. Flow distribution and mass transfer in a parallel microchannel contactor integrated with constructal distributors. *AIChE J* 2010;56:298–317.
- [195] Zhu C, Guo H, Chu C, Fu T, Ma Y. Gas-liquid distribution and mass transfer of CO₂ absorption into sodium glycinate aqueous solution in parallel multi-channel microreactor. *Int J Heat Mass Transf* 2020;157:119943.
- [196] Tondeur D, Fan Y, Commenge J-M, Luo L. Uniform flows in rectangular lattice networks. *Chem Eng Sci* 2011;66:5301–12.
- [197] Tarlet D, Fan Y, Luo L. Design and mixing performance characterization of a mini-channel mixer with nature-inspired geometries. *Chem Eng Res Des* 2020;164:230–9.
- [198] Constantinou A, Gavriilidis A. CO₂ absorption in a microstructured mesh reactor. *Ind Eng Chem Res* 2010;49:1041–9.
- [199] Constantinou A, Barrass S, Pronk F, Brill T, Wenn DA, Shaw JEA, et al. CO₂ absorption in a high efficiency silicon nitride mesh contactor. *Chem Eng J* 2012;207:766–71.
- [200] Zhang S, Lu Y, Gu Y, Zhang X, Sun J, Tang Z. The process intensification of CO₂ absorption in honeycomb fractal reactor fabricated by 3D printer. *Chem Eng Process Intensif* 2018;132:42–7.
- [201] Singh RK, Fu Y, Zeng C, Roy P, Bao J, Xu Z, et al. Hydrodynamics of countercurrent flow in an additive manufactured column with triply periodic minimal surfaces for carbon dioxide capture. *Chem Eng J* 2022:138124.
- [202] Fu Y, Bao J, Wang C, Singh RK, Xu Z, Panagakos G. CFD Study of Countercurrent Flow in Triply Periodic Minimal Surfaces with CO₂BOL Solvent. Pacific Northwest National Lab.(PNNL), Richland, WA (United States); 2019.
- [203] Sithamparam M, Lai LS, Tay WH. Computational fluid dynamics simulation for carbon dioxide gas transport through polydimethylsiloxane membrane with gyroid structure. *Mater Today Proc* 2021;46:1922–8.
- [204] Greco-Coppi M, Hofmann C, Ströhle J, Walter D, Epple B. Efficient CO₂ capture from lime production by an indirectly heated carbonate looping process. *Int J Greenh Gas Control* 2021;112:103430.
- [205] Coppola A, Massa F, Montagnaro F, Scala F. Analysis of the behaviour of limestone sorbents for sorption-enhanced gasification in dual interconnected fluidised bed reactor. *Fuel* 2023;340:127594.